

Bridging Information Asymmetry: A Hierarchical Framework for Deterministic Blind Face Restoration

Zhengjian Yao, Jiakui Hu, Kaiwen Li, Hangzhou He, Xinliang Zhang, Shuang Zeng, Lei Zhu, Yanye Lu

Abstract—Blind face restoration remains a persistent challenge due to the inherent ill-posedness of reconstructing holistic structures from severely constrained observations. Current generative approaches, while capable of synthesizing realistic textures, often suffer from information asymmetry—the intrinsic disparity between the information-sparse low quality inputs and the information-dense high quality outputs. This imbalance leads to a one-to-many mapping, where insufficient constraints result in stochastic uncertainty and hallucinatory artifacts. To bridge this gap, we present Pref-Restore, a hierarchical framework that integrates discrete semantic logic with continuous texture generation to achieve deterministic, preference-aligned restoration. Our methodology fundamentally addresses this information disparity through two complementary strategies: (1) Augmenting Input Density: We employ an auto-regressive integrator to reformulate textual instructions into dense latent queries, injecting high-level semantic stability to constrain the degraded signals; (2) Pruning Output Distribution: We pioneer the integration of on-policy reinforcement learning directly into the diffusion restoration loop. By transforming human preferences into differentiable constraints, we explicitly penalize stochastic deviations, thereby sharpening the posterior distribution toward the desired high-fidelity outcomes. Extensive experiments demonstrate that Pref-Restore achieves state-of-the-art performance across synthetic and real-world benchmarks. Furthermore, empirical analysis confirms that our preference-aligned strategy significantly reduces solution entropy, establishing a robust pathway toward reliable and deterministic blind restoration. The code is available at <https://gitfront.io/r/zjYao/lexW483uvkuL/Pref-Restoration/>

Index Terms—Blind Face Restoration, Information Asymmetry, Auto-Regressive Models, Diffusion Models, On-Policy Reinforcement Learning, Preference Alignment.

I. INTRODUCTION

BLIND Face Restoration (BFR) aims to recover high-quality (HQ) facial images from low-quality (LQ) inputs corrupted by unknown degradations [1]–[7]. Unlike general restoration tasks [8]–[13], BFR is particularly challenging as facial components often occupy limited spatial resolutions in natural scenes, which exacerbates the loss of critical high-frequency information. This extreme information sparsity results in a fundamental information asymmetry: the sparse LQ signals provide insufficient cues to reconstruct dense, identity-consistent details. Consequently, BFR remains a highly ill-posed inverse problem, leading to significant restoration uncertainty.

Zhengjian Yao, Jiakui Hu, Kaiwen Li, Hangzhou He, Xinliang Zhang, Shuang Zeng, Lei Zhu and Yanye Lu are with the Biomedical Engineering Department, College of Future Technology, Peking University, Beijing, China. They are also with the Institute of Medical Technology, Peking University Health Science Center, and the National Biomedical Imaging Center, Peking University, Beijing, China.

Corresponding Authors: Yanye Lu (yanye.lu@pku.edu.cn).

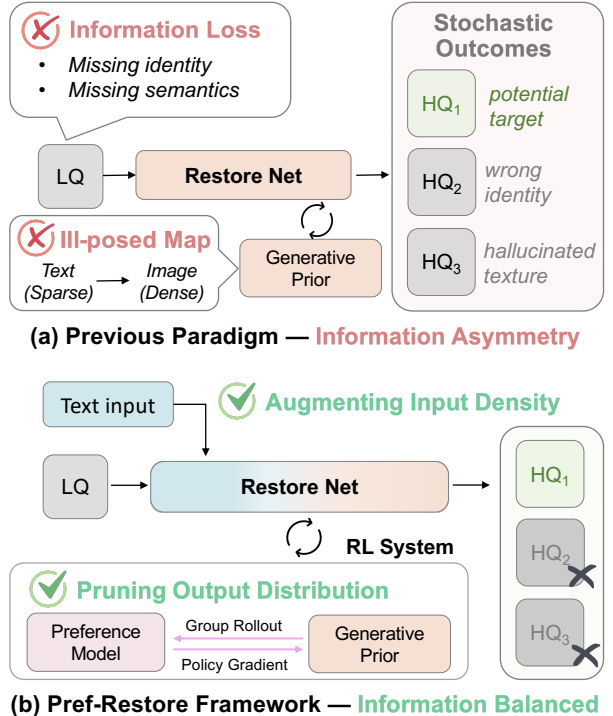


Fig. 1. Conceptual illustration of (a) the conventional generative prior paradigm versus (b) our proposed Pref-Restore framework. Existing methods suffer from information asymmetry, where *ill-posed priors* and *sparse inputs* lead to stochastic outcomes such as hallucinations or identity loss. Our Pref-Restore resolves this by *augmenting input density* through AR-based semantic modeling and *pruning the output distribution* via on-policy reinforcement learning, effectively pruning the uncertain solution space to achieve deterministic, preference-consistent restoration.

Previous restoration paradigms struggle to resolve this asymmetry. Deterministic approaches, typically optimized via pixel-wise objectives, frequently suffer from the “regression-to-the-mean” effect, yielding over-smoothed results [14]–[16]. Conversely, generative priors attempt to address the information ambiguity by constraining the restoration output within a pre-trained generative distribution. However, we argue that this merely shifts the ill-posedness (Fig. 1 (a)): The priors themselves are trained on an ill-posed mapping from sparse semantic signals (such as text or class labels) to dense pixel spaces [17]–[20]. Consequently, the restoration remains prone to stochastic uncertainty and, more critically, to hallucinations that are semantically plausible yet structurally erroneous. Such stochasticity limits the reliability of BFR in identity-sensitive applications, necessitating a more constrained, deterministic restoration framework.

To bridge this information asymmetry and eliminate restora-

tion uncertainty, we propose *Pref-Restore*, a hierarchical framework designed to re-balance the information equation from both ends of the restoration pipeline (Fig. 1 (b)).

First, to augment input density, we employ an Auto-Regressive (AR) integrator as a high-level semantic bridge. It reformulates textual instructions into latent “knowledge queries” via a Next-Token Prediction (NTP) paradigm [21]–[25]. This mechanism is realized through a Multi-modal Knowledge Alignment stage, where we focus on the cross-modal synchronization between discrete linguistic tokens and the continuous diffusion latent space [21], [22], [26]. By internalizing high-level restoration logic (e.g., identifying identity-critical facial components), this stage enables the model to inject stable semantic guidance into degraded signals, effectively mitigating the inherent information sparsity.

Second, to prune the output distribution and ensure deterministic restoration, we integrate On-Policy Reinforcement Learning (RL) directly into the diffusion trajectory [27]–[29]. This is achieved via a Preference-Aware Fine-tuning stage, where we transform subjective human preferences into differentiable constraints. Unlike traditional static fine-tuning, this stage employs a specialized optimization framework to refine the forward diffusion path, using a pre-defined preference model as a “perceptual critic” to penalize stochasticity and prune trajectories that deviate from human aesthetic and fidelity standards. Remarkably, this preference-aligned strategy demonstrates exceptional efficiency, achieving a significant leap in both structural coherence and identity consistency with as few as 30 fine-tuning steps.

The main contributions of this work are summarized as follows:

- **Conceptual Framework:** We identify information asymmetry as the root cause of uncertainty in current BIR models. We propose the Pref-Restore framework, which mitigates this by simultaneously increasing input information density and sharpening the output distribution via preference alignment.
- **SOTA & Controllability:** We provide two optimized variants of Pref-Restore, targeting fidelity and aesthetics respectively. Both variants achieve SOTA performance across multiple benchmarks, offering a superior balance between structural accuracy and visual appeal.
- **Methodological Innovation:** We pioneer the adaptation of on-policy RL specifically for the challenging task of Blind Face Restoration. By treating the multi-step diffusion process as a sequential decision-making trajectory, our method effectively constrains restoration stochasticity through a efficient preference feedback mechanism.

II. RELATED WORKS

A. Blind Face Restoration with Generative Priors

Blind face restoration is an inherently ill-posed problem that necessitates strong auxiliary priors to regularize the solution space, given the unavailability of degradation kernels and identity information. Early attempts primarily exploit geometric priors, such as facial landmarks [30], parsing maps [31], or 3D shapes [32], and reference priors [33], [34] from

guided identity images. However, these methods often falter in real-world scenarios, as estimating accurate geometry from severely degraded inputs is challenging, and high-quality reference images are rarely accessible.

With the advent of deep generative models, recent research has shifted towards leveraging pre-trained generative priors for their superior detail synthesis capabilities. Pioneering works utilizing *StyleGAN* [35], such as *GPEN* [2] and *GPGAN* [1], incorporate structural cues from low-quality inputs to guide the generation process via GAN inversion [36], [37] or spatial feature modulation. To further enhance fidelity, codebook-based priors (e.g., *VQFR* [3] and *CodeFormer* [4]) employ vector-quantized dictionaries to retrieve high-quality texture codes. More recently, diffusion models have also been adapted as refinement modules (e.g., *DR2* [6], *DiffBIR* [11]) to hallucinate high-frequency details. Despite their impressive perceptual quality, these generative approaches fundamentally rely on the accurate mapping from degraded features to the high-quality manifold. This mapping remains fragile under severe degradation, often leading to identity inconsistency or structure-texture misalignment. In contrast, our approach seeks to mitigate these uncertainties by explicitly optimizing the restoration trajectory via task-aware feedback and auxiliary semantic guidance.

B. Text-driven Information Augmentation

The integration of linguistic priors into image restoration has emerged as a promising paradigm to resolve ill-posed reconstruction ambiguities [38]. Textual instructions provide high-level global priors that effectively compensate for the information loss in degraded observations. Unlike conventional methods relying solely on low-level visual features, text-driven approaches leverage semantic descriptions to alleviate the information asymmetry between sparse inputs and dense pixel requirements.

Early attempts primarily utilized pre-trained models like *CLIP* [39] to align degraded features with textual embeddings, providing global semantic constraints. Building upon this, *PromptIR* [40] introduces implicit textual prompts to modulate networks for all-in-one restoration. *InstructIR* [41] further pioneers the use of natural language instructions to drive the restoration process via cross-attention mechanisms, while *DA-CLIP* [42] demonstrates that language can serve as a powerful bridge for multi-task generalization. However, most existing VLM-based methods treat language as a static condition, often failing to dynamically adjust the restoration strategy based on the evolving quality of the intermediate results.

C. Preference-aligned Solution Space Pruning

Traditional image restoration objectives often fail to constrain the high-entropy solution space of generative models, leading to perceptually valid but identity-inconsistent hallucinations. To resolve this, aligning restoration models with human preferences has emerged as a crucial mechanism for solution space pruning.

Early explorations utilized RL for toolchain selection, such as *RL-Restore* [43] and *Path-Restore* [44]. Inspired by the success of RLHF [45], recent research has shifted toward

fine-grained perceptual alignment. *DiffusionReward* [46] utilizes learned reward models to provide dense supervision, addressing over-smoothing artifacts. To bypass explicit reward modeling, Direct Preference Optimization (DPO) [47] and its variants like *DSPO* [48] integrate semantic feedback to rectify artifacts. More recently, advanced RL algorithms such as Group Relative Policy Optimization (GRPO) [27] have been adapted in frameworks like *IRPO* [49], *RealSR-R1* [50], and *TTPO* [51] to enhance online preference exploration.

In the context of BFR, we argue that preference alignment should serve as a distribution sharpening mechanism. By leveraging on-policy RL via the DiffusionNFT [29] framework, our approach explicitly prunes suboptimal generative modes, ensuring the restoration remains anchored to a preference-aligned, high-fidelity manifold.

III. FOUNDATIONS OF DISTRIBUTION PRUNING

The fundamental information asymmetry in BFR results in a one-to-many mapping, where a single sparse input can correspond to multiple semantically plausible but structurally inconsistent outputs. To eliminate this stochastic uncertainty and ensure deterministic restoration, it is essential to prune the generative solution space, guiding the model's posterior distribution toward a high-fidelity manifold that aligns with human preferences.

To this end, we leverage the principles of DiffusionNFT [29], [52] as our mathematical foundation. DiffusionNFT bypasses the complexities of policy gradients on the reverse process by performing RL directly on the forward diffusion process. Instead of optimizing likelihood ratios of a discretized reverse policy, it refines the diffusion dynamics through the velocity field that parameterizes the forward process.

Specifically, given a pretrained diffusion policy π_{old} and a scalar reward $r(x_0, c) \in [0, 1]$ defined on generated samples, DiffusionNFT induces two implicit data distributions:

$$\pi^+(x_0 | c) \propto r(x_0, c) \pi_{\text{old}}(x_0 | c), \quad (1)$$

$$\pi^-(x_0 | c) \propto (1 - r(x_0, c)) \pi_{\text{old}}(x_0 | c). \quad (2)$$

In the context of restoration, π^+ represents the desired high-fidelity distribution, while π^- captures failure modes such as over-smoothing or identity-inconsistent hallucinations. By explicitly modeling these negative samples, policy improvement is formulated as a contrastive refinement between positive and negative generations. Under the velocity parameterization, let v_{old} , v^+ , and v^- denote the velocity fields associated with π_{old} , π^+ , and π^- , respectively. A stable policy improvement direction $\Delta(x_t, t)$ is then expressed as:

$$\begin{aligned} \Delta(x_t, t) &= \alpha(x_t)(v^+(x_t, t) - v_{\text{old}}(x_t, t)) \\ &= (1 - \alpha(x_t))(v_{\text{old}}(x_t, t) - v^-(x_t, t)), \end{aligned} \quad (3)$$

where $\alpha(x_t) \in [0, 1]$ balances the attraction toward positive restorations and the repulsion from negative artifacts.

To achieve this without training separate models for v^+ and v^- , we optimize a single network v_θ via an implicit supervised objective:

$$\begin{aligned} \mathcal{L}_{\text{NFT}}(\theta) &= \mathbb{E} \left[r \|v_\theta^+(x_t, t) - v\|_2^2 \right. \\ &\quad \left. + (1 - r) \|v_\theta^-(x_t, t) - v\|_2^2 \right], \end{aligned} \quad (4)$$

where v is the ground-truth velocity, and the implicit velocities are constructed as $v_\theta^+ = (1 - \gamma)v_{\text{old}} + \gamma v_\theta$ and $v_\theta^- = (1 + \gamma)v_{\text{old}} - \gamma v_\theta$. This formulation provides the necessary mechanism to internalize solution boundaries and achieve preference-aligned, deterministic restoration.

IV. METHODOLOGY

To address the inherent information asymmetry and recursive ill-posedness in blind face restoration, we propose **Pref-Restore**. Our framework orchestrates the strengths of discrete semantic modeling and continuous texture generation to achieve a deterministic and preference-aligned restoration. In the following sections, we first reformulate the restoration problem through the lens of information rebalance [53] (Sec. IV-A), followed by the detailed hierarchical architecture (Sec. IV-B) and our two-stage training paradigm (Sec. IV-C).

A. Overview: Re-balancing the Information Equation

Conventional Blind Image Restoration is formulated as the estimation of a HQ image $x \in \mathcal{X}$ from a degraded observation $y = \mathcal{D}(x) + \epsilon$, where $\mathcal{D}(\cdot)$ denotes an unknown degradation function. From a Bayesian perspective, this is a Maximum A Posteriori (MAP) estimation problem:

$$\begin{aligned} \hat{x}_{\text{MAP}} &= \arg \max_x \log p(x|y) \\ &= \arg \max_x (\log p(y|x) + \log p(x)), \end{aligned} \quad (5)$$

where $p(y|x)$ is the likelihood term representing data fidelity, and $p(x)$ is the prior term capturing the statistics of natural images. Due to the severe loss of high-frequency information in y , the conditional entropy $H(x|y)$ is excessively high, resulting in a highly diffused solution space prone to uncertainty. This disparity between sparse inputs and dense pixel-wise restoration constitutes the information asymmetry that leads to stochastic hallucinations.

We argue that relying solely on a generic generative prior to regularize this process is insufficient, as the mapping from sparse semantics to dense pixels remains under-determined. To resolve this, Pref-Restore re-balances the objective by simultaneously augmenting the conditional context and constraining the output distribution. Formally, we seek the optimal restoration \hat{x} by maximizing a joint objective:

$$\hat{x} = \arg \max_x \left(\underbrace{\log p(x|y, \mathcal{S}_{\text{AR}})}_{\text{Augmented Likelihood}} + \lambda \cdot \underbrace{\mathcal{R}_{\text{pref}}(x)}_{\text{Preference Constraint}} \right), \quad (6)$$

where λ is a balancing coefficient. The preference term $\mathcal{R}_{\text{pref}}(x)$ can be interpreted as an energy-based prior [54] $p_{\text{pref}}(x) \propto \exp(\mathcal{R}_{\text{pref}}(x))$, which re-weights the probability distribution of the sampling trajectory. This formulation effectively steers the reverse diffusion process toward a human-aligned, high-fidelity manifold while pruning off-target stochastic modes. Our strategy operates on two fronts:

- **Input Information Augmentation:** We introduce an AR module to integrate high-level textual semantics T . By modeling the discrete semantic distribution $p(s|T, y)$,

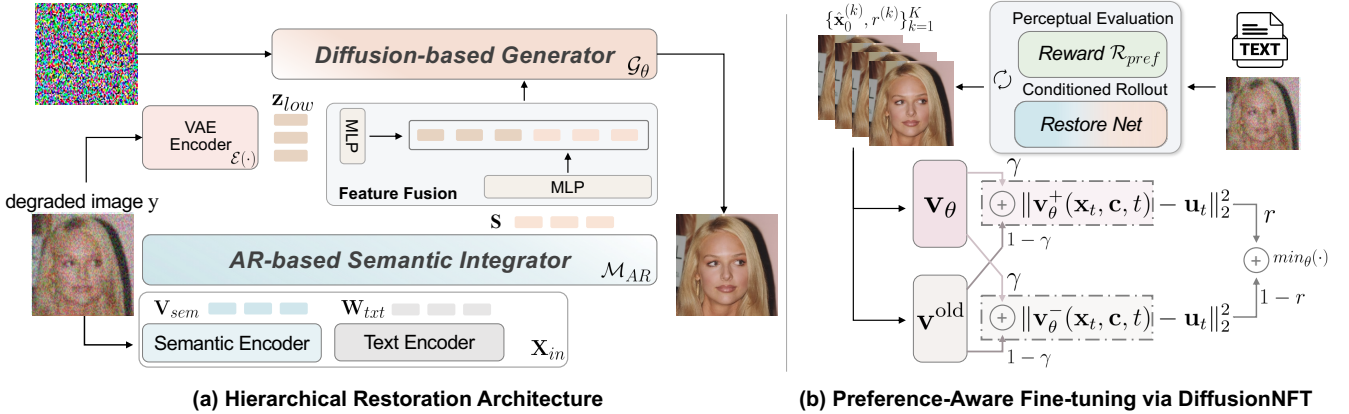


Fig. 2. **The overall framework of Pref-Restore.** (a) **Hierarchical Restoration Architecture:** Our model decouples the blind face restoration task into a discrete semantic stream and a continuous texture stream. The *AR-based Semantic Integrator* processes degraded observations y and textual instructions T to generate discrete semantic tokens S via Next-Token Prediction (NTP), acting as a global structural anchor. Simultaneously, the *Continuous Diffusion-based Generator* leverages these semantic anchors and low-level texture latents z_{low} to reconstruct high-fidelity details through a conditional flow matching process. (b) **Preference-Aware Fine-tuning via DiffusionNFT:** To eliminate hallucinations, we employ an on-policy RL strategy. The current policy v_θ performs a group rollout to generate K candidates, evaluated by a frozen reward model \mathcal{R}_{pref} . Based on the normalized rewards r , we construct implicit positive (v_θ^+) and negative (v_θ^-) velocity proxies. The model is optimized by contrasting these proxies against the forward data flow, rotating the vector field toward the preference-aligned manifold.

we derive a dense semantic representation \mathcal{S}_{AR} that enriches the degraded input. According to the principle of information gain, this effectively shrinks the uncertainty of the posterior:

$$H(x|y, \mathcal{S}_{AR}) \leq H(x|y). \quad (7)$$

• **Output Distribution Sharpening:** To prune the remaining stochasticity, we employ an On-Policy RL mechanism that optimizes the model via the preference reward $\mathcal{R}_{pref}(x)$. By treating the sequential diffusion process as a policy-guided trajectory, this mechanism effectively “sharpens” the generative distribution, steering the model from producing multiple plausible hallucinations toward a unique, deterministic, and faithful outcome.

By transforming the restoration task from a simple prior-constrained mapping into a dual-ended optimization process, Pref-Restore systematically mitigates the uncertainty inherent in generative restoration.

B. Hierarchical Architecture: Bridging Discrete Logic and Continuous Textures

The core of Pref-Restore is a hierarchical architecture designed to decouple global semantic reasoning from local texture synthesis, thereby resolving the Information Asymmetry between sparse inputs and dense outputs. As illustrated in Fig. 2 (a), our framework comprises two synergistic components: an AR-based Semantic Integrator for high-level semantic modeling and a continuous Diffusion-based Generator for high-fidelity reconstruction.

1) **AR-based Semantic Integrator:** The AR module aims to eliminate semantic ambiguity by operating in a discrete token space. Given a degraded image $y \in \mathbb{R}^{H \times W \times 3}$ and its corresponding textual description T , we first extract their respective multimodal features. Specifically, a semantic encoder (e.g., Siglip2), denoted as $\Phi_{sem}(\cdot)$, projects the degraded image into a continuous visual embedding space $\mathbf{V}_{sem} =$

$\Phi_{sem}(y) \in \mathbb{R}^{L \times C}$, where L and C denote the sequence length and embedding dimension, respectively. Simultaneously, the textual instruction T is transformed into text embeddings \mathbf{W}_{txt} via a text encoder.

The input to the AR model (e.g., Qwen3) is formed by the concatenation of these multimodal representations: $\mathbf{X}_{in} = [\mathbf{V}_{sem}; \mathbf{W}_{txt}]$. To bridge the gap between continuous signals and discrete logic, the AR module \mathcal{M}_{AR} models the restoration task through a NTP paradigm over a learned visual vocabulary \mathcal{V} . Formally, it generates a sequence of discrete semantic tokens $S = \{s_1, s_2, \dots, s_n\}$, where each token $s_i \in \mathcal{V}$ is sampled from the predicted categorical distribution:

$$P(s_i | s_{<i}, \mathbf{X}_{in}) = \text{Softmax}(\mathcal{M}_{AR}(s_{<i}, \mathbf{X}_{in})). \quad (8)$$

These discrete tokens S serve as a “semantic anchor,” encapsulating high-level attributes (e.g., facial identity, structural layout) that remain invariant to pixel-level degradations.

2) **Continuous Diffusion-based Generator:** While the AR module provides global logic, the Diffusion module \mathcal{G}_θ translates these priors into fine-grained textures. To compensate for the potential loss of fine-grained structures in discrete tokens, we explicitly incorporate low-level texture cues $z_{low} = \mathcal{E}(y)$, where $\mathcal{E}(\cdot)$ is a pre-trained VAE encoder.

The restoration is modeled as a Conditional Flow Matching process. We seek to learn a velocity field v_θ that defines a probability path between the noise distribution and the high-fidelity latent manifold. For any timestep $t \in [0, 1]$, the generative trajectory is defined by the ODE:

$$d\mathbf{z}_t = v_\theta(\mathbf{z}_t, t, \mathbf{S}, z_{low})dt. \quad (9)$$

The DiT architecture estimates v_θ by synergizing the global semantic “anchor” S and the local structural “prior” z_{low} .

3) **Structural Synergies:** By decomposing the problem into discrete semantic logic S and continuous texture latents z_{low} , Pref-Restore achieves a dual-stream optimization. The discrete stream acts as an “information densifier” to recover missing

semantics, while the continuous stream ensures the final output $\hat{x} = \mathcal{D}_{vae}(\mathbf{z}_0)$ satisfies the perceptual granularity required for high-fidelity restoration.

C. Training Strategy: Knowledge Alignment and Preference Optimization

Pref-Restore is trained via a progressive two-stage paradigm to transition from general generation to deterministic restoration. *Multi-modal Knowledge Alignment* synchronizes textual instructions from the AR integrator and VAE-encoded texture features with the diffusion latent space, bridging discrete reasoning and continuous synthesis. *Preference-Aware Fine-tuning* then employs a preference model as a perceptual critic to compress the diffusion prior. By pruning the stochastic solution space, this stage ensures the restoration converges toward a deterministic output aligned with human aesthetic and identity expectations.

1) **Stage 1: Multi-modal Knowledge Alignment.** The first training stage aims to establish a shared latent manifold between discrete semantic reasoning and continuous image reconstruction. We divide this process into two synergistic objectives: *Semantic-to-Diffusion Alignment* and *Texture-to-Diffusion Alignment*.

Stage1.1 Semantic-to-Diffusion Alignment. To bridge the modality gap, we freeze the backbone of the Diffusion model \mathcal{G}_θ and exclusively optimize the AR module \mathcal{M}_{AR} and a dedicated cross-modal projector \mathcal{P} . The optimization objective is formulated as a joint loss:

$$\mathcal{L}_{align} = \mathcal{L}_{CE} + \alpha \mathcal{L}_{diff}, \quad (10)$$

where \mathcal{L}_{CE} is the cross-entropy loss for Next-Token Prediction over the expanded visual vocabulary $\mathcal{V}_{img} = \{\langle I_0 \rangle, \dots, \langle I_{65535} \rangle\}$. The second term, \mathcal{L}_{diff} , is the standard diffusion denoising loss. Crucially, gradients from \mathcal{L}_{diff} are backpropagated through the frozen \mathcal{G}_θ to the projector \mathcal{P} and \mathcal{M}_{AR} . This ensures that the generated semantic tokens \mathbf{S} are not only semantically accurate but also numerically aligned with the Diffusion module's cross-attention subspace.

Stage1.2 Texture-to-Diffusion Alignment. Once the semantic space is aligned, we freeze \mathcal{M}_{AR} and fine-tune both the VAE encoder \mathcal{E} and the Diffusion backbone \mathcal{G}_θ . This substage is designed to let the model internalize low-level texture cues \mathbf{z}_{low} . To proactively mitigate degradations at the latent level, we introduce a latent-level consistency loss:

$$\mathcal{L}_{mse} = \|\mathcal{E}(y) - \mathcal{E}(x)\|_2^2, \quad (11)$$

where y and x denote the degraded and ground-truth images, respectively. Although fine-tuning \mathcal{G}_θ slightly constrains the stochastic diversity of the pre-trained model, it significantly enhances structural fidelity by prioritizing the deterministic conditioning signals from \mathbf{z}_{low} . The total objective for this stage is $\mathcal{L}_{stage1} = \mathcal{L}_{diff} + \beta \mathcal{L}_{mse}$.

2) **Stage 2: Preference-Aware Fine-tuning via Forward Flow Contrast.** While Stage 1 aligns the semantic spaces, the generative prior may still yield hallucinations or inconsistent identities due to the stochastic nature of the diffusion process. To strictly align the restoration quality with human perceptual

standards, we adapt the principles of DiffusionNFT [29]. We treat the restoration process as a conditional policy optimization problem, where the goal is to navigate the flow trajectory towards a preference-optimal manifold $\mathcal{X}_{pref} \subset \mathcal{X}$.

As outlined in Fig. 2 (b), the training iterates through a feedback-driven cycle:

Conditioned Rollout and Perceptual Evaluation. For a given condition $\mathbf{c} = (\mathbf{S}, \mathbf{z}_{low})$, we sample K candidate latent restorations $\{\hat{\mathbf{x}}_0^{(k)}\}_{k=1}^K \sim \pi_\theta$. These are evaluated by \mathcal{R}_{pref} to yield normalized optimality probabilities $r^{(k)} \in [0, 1]$ via group centering and clipping:

$$r^{(k)} = 0.5 + 0.5 \cdot \text{clip}\left(\frac{r_{(k)}^{\text{raw}} - \mu_{group}}{Z}, -1, 1\right), \quad (12)$$

where μ_{group} is the mean reward of the current rollout batch, and Z is a scaling factor. Here, $r^{(k)} \rightarrow 1$ signifies a high-fidelity restoration (positive exemplar), while $r^{(k)} \rightarrow 0$ indicates a failed restoration (negative exemplar).

Implicit Velocity Proxies. To guide the update without expensive ODE back-propagation, we define implicit positive (\mathbf{v}_θ^+) and negative (\mathbf{v}_θ^-) velocity proxies:

$$\mathbf{v}_\theta^+(\mathbf{x}_t) := (1 - \gamma)\mathbf{v}^{\text{old}}(\mathbf{x}_t, \mathbf{c}, t) + \gamma\mathbf{v}_\theta(\mathbf{x}_t, \mathbf{c}, t), \quad (13)$$

$$\mathbf{v}_\theta^-(\mathbf{x}_t) := (1 + \gamma)\mathbf{v}^{\text{old}}(\mathbf{x}_t, \mathbf{c}, t) - \gamma\mathbf{v}_\theta(\mathbf{x}_t, \mathbf{c}, t). \quad (14)$$

Intuitively, \mathbf{v}_θ^+ reinforces the trajectory deviations that lead to higher fidelity (exploiting success), while \mathbf{v}_θ^- penalizes directions associated with artifacts (suppressing failure).

Preference-Weighted Optimization. The training objective minimizes the contrastive flow matching loss, ensuring the policy rotates towards high-reward data flows:

$$\begin{aligned} \mathcal{L}_{RL} = \mathbb{E}_{\substack{\mathbf{x}_t \sim \mathcal{U}(0,1) \\ \hat{\mathbf{x}}_0 \sim \pi_\theta, \mathbf{c}}} & \left[r \|\mathbf{v}_\theta^+(\mathbf{x}_t, \mathbf{c}, t) - \mathbf{u}_t\|_2^2 \right. \\ & \left. + (1 - r) \|\mathbf{v}_\theta^-(\mathbf{x}_t, \mathbf{c}, t) - \mathbf{u}_t\|_2^2 \right], \end{aligned} \quad (15)$$

where \mathbf{u}_t is the target forward velocity. This mechanism effectively prunes the solution space of low-quality textures by suppressing “negative” trajectories through the $1 - r$ term.

V. EXPERIMENTS

A. Experimental Settings

Implementation Details. We initialize our Pref-Restore with the weights of *blip-3o-next* [22] to leverage its pre-aligned multi-modal features. In the AR-based semantic integrator, we employ *Siglip2* [55] as the semantic encoder Φ_{sem} . The degraded images are resized to 384×384 before being fed into a lightweight *Qwen3-0.6B* backbone. During the NTP process, the model learns to predict 729 tokens from a visual vocabulary \mathcal{V}_{img} of size 65,536, which serve as high-level semantic anchors. For the generative component, we adopt the *SANA-1.5_1.6B* [56] as our Diffusion-based module due to its efficiency and high fidelity.

Unlike the original *blip-3o-next*, we tailor our framework for image restoration through a three-step pipeline (Sec. IV-C): (1) Stage 1.1: Semantic-to-Diffusion Alignment; (2) Stage 1.2: Texture-aware Feature Refinement; and (3) Stage 2: Preference-Aware Fine-tuning via DiffusionNFT. The detailed

TABLE I
TRAINING RECIPE OF PREF-RESTORE.

Hyperparameters	Stage-1.1 (Step1)	Stage-1.2 (Step2)	Stage-2
Learning rate	1×10^{-5}	1×10^{-5}	3×10^{-4}
LR scheduler	Cosine	Cosine	Constant
Weight decay	0.0	0.0	1×10^{-4}
Optimizer	AdamW ($\beta_1 = 0.9, \beta_2 = 0.999, \epsilon = 1 \times 10^{-8}$)		
Loss type	CE+MSE(diff)	MSE(VAE+diff)	MSE(diff)
Warm-up ratio	0.01	0.01	0
Batch size	128	128	72
Module	Qwen3	SANA+VAE	SANA

training hyperparameters and schedules are summarized in Table I. All experiments were implemented using PyTorch and conducted on a server with 8 NVIDIA A100 GPUs.

Datasets. Following the common practice in blind face restoration [1], [2], [4], we use the FFHQ dataset [57] (70,000 high-quality images) for training. All images are resized to 512×512 . To synthesize degraded images, we utilize the following degradation model:

$$I_l = \{[(I_h \otimes k_\sigma) \downarrow_r + n_\delta]_{\text{JPEG}_q}\} \uparrow_r, \quad (16)$$

where $\sigma \in [1, 15]$, $r \in [1, 30]$, $\delta \in [0, 20]$, and $q \in [40, 100]$ are randomly sampled to simulate complex real-world artifacts.

For evaluation, we utilize one synthetic and four real-world datasets:

- CelebA-Test: A synthetic dataset comprising 3,000 images from CelebA-HQ [58], with LQ versions generated via Eq. (16).
- LFW-Test [59]: 1,711 mildly degraded real-world images (one per individual).
- WIDER-Test [60]: 970 heavily degraded real-world images from the WIDER Face dataset.
- WebPhoto-Test [1]: 407 real-world face images collected from the internet, including historical photos that exhibit complex and severe degradations.
- CelebChild-Test [1]: 180 child faces of celebrities, exhibiting unique degradation and cross-age patterns.

Evaluation Metrics. To provide comprehensive evaluations, we categorize our metrics into general image quality and face-specific fidelity assessment. For general quality, we employ reference-based metrics including LPIPS [61] and FID [62], alongside no-reference metrics for perceptual quality such as MUSIQ [63], CLIPQA+ [64], and MANIQA [65].¹

For face-specific fidelity, we adopt the ArcFace embedding angle (Deg) and Landmark Distance (LMD) [66] to evaluate identity preservation and structural accuracy. Additionally, we use topiq_nr-face, topiq_nr_swin-face, and DSL-FIQA as specialized no-reference metrics to quantify the aesthetic and biological plausibility of the restored faces.²

B. Quantitative Comparison

Results on Synthetic Datasets. We conduct a comprehensive comparison between our Pref-Restore and several SOTA

¹We exclude PSNR and SSIM, as they tend to penalize high-frequency generative details in severely degraded scenarios, often yielding misleadingly high scores for over-smoothed results.

²These metrics are implemented based on the IQA-PyTorch toolbox [67].

methods, including diffusion-based approaches (DR2 [6], DiffFace [5], and DiffBIR [11]), GAN-based models (GPGAN [1], GPEN [2]), and VQ-based techniques (CodeFormer [4], VQFR [3], RestoreFormer++ [68], and DAEFR [7]).

As summarized in Table II, we evaluate two distinct variants of our framework: *Pref-Restore Fidelity* (after stage 1) and *Pref-Restore Quality* (after stage 2). This dual-model analysis provides a comprehensive perspective on how our hierarchical strategies progressively resolve the BFR challenge.

Regarding identity and structural fidelity, *Pref-Restore Fidelity* achieves the best performance in face-specific fidelity metrics, including LMD (5.1337) and ArcFace Deg (54.0623). This superior performance validates the efficacy of our AR-based semantic integrator and texture-aware refinement. By establishing robust structural anchors at the early stage, these components prevent the generative process from drifting, ensuring that the reconstructed details remain strictly consistent with the original identity despite severe input degradation.

The impact of preference-aware fine-tuning is most evident in the perceptual and aesthetic dimensions. After stage 2, *Pref-Restore Quality* dominates across all no-reference quality metrics, achieving peak scores in MUSIQ (76.3296), CLIPQA+ (0.6997), and topiq-swin (0.9002). The substantial gains in aesthetic-related indices, such as DSL-FIQA, demonstrate that the DiffusionNFT mechanism effectively regularizes the diffusion vector field. By prioritizing high-reward, artifact-free trajectories, this stage successfully bridges the gap between mere pixel-level reconstruction and high-level, preference-aligned restoration.

Furthermore, both variants demonstrate exceptional distribution alignment with the high-quality manifold, as evidenced by significantly lower FID scores compared to existing methods. In particular, *Pref-Restore Fidelity* achieves an FID (FFHQ) of 16.2435. This result indicates that our hierarchical architecture does not sacrifice overall image realism for structural accuracy; instead, it successfully maps restored images onto the high-quality distribution while maintaining the deterministic constraints necessary for faithful face restoration.

Discussion on the Fidelity-Quality Trade-off. The results in Table II empirically validate the trade-off inherent in generative restoration. While *Fidelity* models focus on minimizing landmark and identity distance, they may slightly sacrifice pure aesthetic scores. Conversely, our *Quality* variant, optimized via DiffusionNFT, pushes the boundaries of visual realism. By providing these two variants, *Pref-Restore* offers a flexible solution that can be adapted to different downstream applications, such as forensic identification (Fidelity-oriented) or social media enhancement (Quality-oriented).

Scaling Analysis and Distribution Alignment. To investigate the distribution alignment capability of *Pref-Restore*, we monitor the evolution of FID across different training phases, as illustrated in Fig. 3. A pivotal observation is the continuous and significant decline of FID scores throughout Stage 1.

Specifically, during *Semantic-to-Diffusion Alignment*, the FID score drops sharply as the model establishes the mapping between discrete semantic logic and the generative latent space. In *Texture-to-Diffusion Alignment*, the FID continues to decrease steadily as the model internalizes fine-grained

TABLE II

QUANTITATIVE COMPARISON ON THE SYNTHETIC CELEBA-TEST DATASET. WE REPORT TWO VARIANTS OF OUR FRAMEWORK: **PREF-RESTORE FIDELITY** (OPTIMIZED FOR IDENTITY PRESERVATION IN STAGE I) AND **PREF-RESTORE QUALITY** (OPTIMIZED FOR PERCEPTUAL AESTHETICS VIA DIFFUSIONNFT IN STAGE II). **RED** AND **BLUE** COLORS INDICATE THE BEST AND THE SECOND-BEST PERFORMANCE, RESPECTIVELY.

CelebA-Test Methods	General Image Quality Evaluation					Face Image Quality Evaluation					
	LPIPS↓	FID(HQ)↓	FID(FFHQ)↓	MUSIQ↑	CLIPQA↑	MANIQA↑	LMD↓	Deg↓	topiq↑	topiq-swin↑	DSL-FIQA↑
GFGAN	0.4315	21.7414	53.4286	75.3721	0.6529	0.5737	5.1382	58.0687	0.8018	0.8559	0.8838
GPEN	0.4359	33.2368	49.9732	74.9878	0.6031	0.4375	5.9907	59.8849	0.668	0.7927	0.7275
DR2	0.4599	48.7970	76.1381	63.8542	0.5233	0.5021	6.5405	66.7169	0.6507	0.7348	0.7108
DifFace	0.4389	18.7722	47.3185	66.7451	0.5570	0.4975	5.4759	63.4511	0.6730	0.7560	0.7581
RestoreFormer++	0.4763	45.0251	43.0445	72.3612	0.6220	0.5687	8.8019	70.5083	0.7319	0.7955	0.8301
DAEFR	0.4317	20.9941	48.0317	74.5893	0.6738	0.5761	5.6332	62.8184	0.7851	0.8380	0.8580
Codeformer	0.4005	27.4670	65.4874	75.9432	0.6584	0.5527	5.3819	62.1972	0.7946	0.8436	0.8688
VQFR	0.4095	20.5485	54.2846	73.2969	0.6316	0.5531	5.7297	62.2595	0.7764	0.8239	0.8567
Pref-Restore Fidelity	0.4175	16.2435	40.7014	74.1902	0.6526	0.4895	5.1337	54.0623	0.7471	0.8298	0.8246
Pref-Restore Quality	0.5099	18.1590	40.2627	76.3296	0.6997	0.5810	8.3588	73.9882	0.8227	0.9002	0.9002

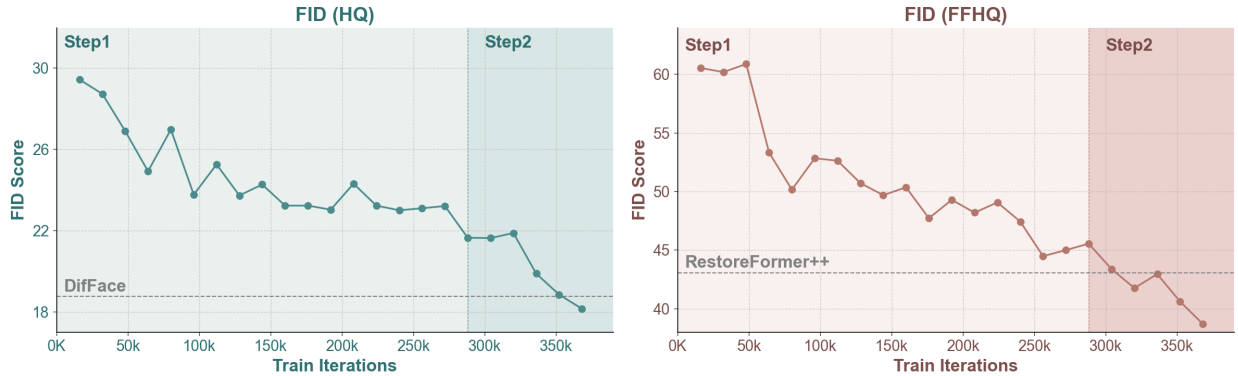


Fig. 3. **Evolution of FID scores during the hierarchical training process.** The curves illustrate the FID (HQ) and FID (FFHQ) results on the CelebA-Test dataset. Stage 1 comprises two critical steps: Step 1 (Semantic-to-Diffusion Alignment) and Step 2 (Texture-to-Diffusion Alignment). The sustained decrease in FID during Stage 1 highlights the scaling effect of our AR-based semantic integrator in aligning distributions. Our framework consistently maintains a downward trajectory, eventually outperforming strong baselines like DiffFace and RestoreFormer++ by a clear margin.

texture priors z_{low} . By the end of Stage 1, *Pref-Restore* already surpasses established SOTA methods such as *DifFace* and *RestoreFormer++*, demonstrating the superior distribution alignment inherited from the scaling effect of our AR-based semantic integrator.

Results on Real-World Datasets. To further validate the generalization and robustness of *Pref-Restore*, we conduct extensive evaluations on four representative real-world datasets: LFW-Test, WebPhoto-Test, WIDER-Test, and CelebChild-Test. These datasets contain diverse and complex degradations that significantly differ from the synthetic training distribution. The quantitative results are summarized in Tables III - VI.

Our framework consistently outperforms SOTA methods across nearly all no-reference quality and face-specific metrics, demonstrating robust generalization in real-world scenarios. The aesthetic superiority of *Pref-Restore* is particularly evident across all four benchmark datasets, where it achieves peak scores in MUSIQ, CLIPQA+, and MANIQA. On the heavily degraded WIDER-Test, our method leads by a substantial margin—for instance, reaching 0.6913 in CLIPQA compared to 0.6437 for the second-best method. This significant gain validates that the preference-aware fine-tuning in stage 2 effectively regularizes the model to generate results that align with high-quality human visual perception, even under extreme noise and blur.

The framework also exhibits superior facial plausibility, dominating face-specific quality indices such as topiq and DSL-FIQA. This advantage is most pronounced on the

CelebChild-Test dataset, which involves unique cross-age facial features that typically challenge conventional models. *Pref-Restore* reaches a DSL-FIQA of 0.8859, significantly surpassing GAN-based (e.g., GFGAN) and VQ-based (e.g., CodeFormer) approaches. This suggests that the AR-based semantic integrator successfully captures invariant facial priors, enabling the model to reconstruct structurally sound and semantically plausible features that generalize across different ages and severe artifacts.

Beyond individual quality metrics, our model demonstrates exceptional distribution robustness and visual clarity. While certain diffusion-based methods, such as *DifFace*, may exhibit lower FID on specific datasets due to conservative sampling, *Pref-Restore* maintains highly competitive FID scores while providing markedly better edge sharpness and identity details. These results confirm that our hierarchical architecture successfully avoids the over-smoothing trap common in traditional restoration paradigms. Instead, by pruning the generative space, *Pref-Restore* navigates toward a “sharp and faithful” manifold, ensuring that the restored images are both perceptually vivid and structurally accurate.

C. Qualitative Evaluation on Synthetic Datasets

We first conduct a qualitative comparison on the CelebA-HQ [58] dataset to evaluate the restoration performance under controlled synthetic degradations. Fig. 4 illustrates the results of our *Pref-Restore* against several state-of-the-art methods,

TABLE III

QUANTITATIVE COMPARISON ON THE REAL-WORLD LFW-TEST DATASET. THIS DATASET REPRESENTS MILD REAL-WORLD DEGRADATIONS. *Pref-Restore* DEMONSTRATES SUPERIOR PERFORMANCE IN BOTH NATURAL AND FACE-SPECIFIC QUALITY METRICS, ACHIEVING THE BEST PERCEPTUAL ALIGNMENT. **RED** AND **BLUE** INDICATE BEST AND SECOND-BEST RESULTS.

LFW-Test Methods	Natural Image Quality Evaluation				Face Image Quality Evaluation		
	FID↓	MUSIQ↑	CLIPQA+↑	MANIQA↑	topiq↑	topiq-swin↑	DSL-FIQA↑
GFPGAN	48.6610	76.5157	0.6630	0.5843	0.8217	0.8765	0.8811
GPEN	55.0946	72.3826	0.5946	0.4606	0.7308	0.8191	0.7863
DR2	53.5473	72.4804	0.5970	0.5308	0.7481	0.8156	0.8231
DifFace	47.0041	69.8269	0.5642	0.4600	0.6727	0.7613	0.7554
RestoreFormer	49.3172	73.6487	0.6160	0.5657	0.7464	0.8043	0.8325
DAEFR	48.5389	75.8789	0.6559	0.5425	0.7744	0.8369	0.8365
Codeformer	52.4015	75.4539	0.6480	0.5231	0.7787	0.8404	0.8431
VQFR	50.9369	74.5095	0.6077	0.5353	0.7617	0.8257	0.8352
Pref-Restore	54.7887	76.6660	0.6951	0.5883	0.8471	0.9121	0.8913

TABLE IV

QUANTITATIVE COMPARISON ON THE REAL-WORLD WEBPHOTO-TEST DATASET. EVALUATION ON COMPLEX, HISTORICAL INTERNET PHOTOS. OUR METHOD EXHIBITS ROBUST GENERALIZATION, PARTICULARLY IN HIGH-LEVEL AESTHETIC METRICS (MUSIQ/CLIPQA), OUTPERFORMING BOTH VQ-BASED AND GAN-BASED BASELINES. **RED** AND **BLUE** INDICATE BEST AND SECOND-BEST RESULTS.

Webphoto-Test Methods	Natural Image Quality Evaluation				Face Image Quality Evaluation		
	FID↓	MUSIQ↑	CLIPQA+↑	MANIQA↑	topiq↑	topiq-swin↑	DSL-FIQA↑
GFPGAN	91.7843	74.7166	0.6157	0.5366	0.7622	0.8146	0.8152
GPEN	86.5962	65.6675	0.4886	0.4290	0.6466	0.7339	0.7094
DR2	123.5743	64.1698	0.5038	0.4510	0.6160	0.6946	0.6669
DifFace	82.6670	65.5357	0.4940	0.4236	0.5924	0.6900	0.6647
RestoreFormer	79.6334	69.8371	0.5430	0.5183	0.6653	0.7337	0.7267
DAEFR	77.4463	72.7081	0.5944	0.5140	0.7029	0.7695	0.7705
Codeformer	92.6693	71.9399	0.5930	0.4831	0.7079	0.7665	0.8279
VQFR	88.3393	70.9087	0.5675	0.4909	0.6994	0.7534	0.7601
Pref-Restore	85.5779	76.0059	0.7035	0.5384	0.7837	0.8506	0.8486

TABLE V

QUANTITATIVE COMPARISON ON THE REAL-WORLD WIDER-TEST DATASET. FOR HEAVILY DEGRADED FACES, *Pref-Restore* ACHIEVES SIGNIFICANT GAINS IN FID AND ALL FACE QUALITY ASSESSMENTS, DEMONSTRATING THE EFFECTIVENESS OF THE DIFFUSIONNFT-ALIGNED VECTOR FIELD IN HANDLING EXTREME ARTIFACTS. **RED** AND **BLUE** INDICATE BEST AND SECOND-BEST RESULTS.

Wilder-Test Methods	Natural Image Quality Evaluation				Face Image Quality Evaluation		
	FID↓	MUSIQ↑	CLIPQA+↑	MANIQA↑	topiq↑	topiq-swin↑	DSL-FIQA↑
GFPGAN	42.9806	74.8329	0.6431	0.5551	0.7949	0.8546	0.8556
GPEN	55.4026	75.5878	0.6037	0.4459	0.7166	0.8224	0.7600
DR2	54.8225	65.3340	0.5254	0.4751	0.6792	0.7560	0.7401
DifFace	38.4898	65.0191	0.5377	0.4326	0.6406	0.7367	0.7131
RestoreFormer	51.3830	67.8415	0.5644	0.4984	0.6707	0.7544	0.7532
DAEFR	37.6716	74.1470	0.6437	0.5204	0.7476	0.8151	0.8134
Codeformer	37.6606	71.8923	0.6160	0.4816	0.7316	0.7993	0.7977
VQFR	38.8920	71.4168	0.5901	0.5043	0.7317	0.7977	0.8024
Pref-Restore	35.1473	76.2551	0.6913	0.5828	0.8431	0.9020	0.8892

TABLE VI

QUANTITATIVE COMPARISON ON THE REAL-WORLD CELEBCCHILD-TEST DATASET. TESTING THE MODEL'S ABILITY TO RESTORE CHILD FACES. THE LEADING SCORES IN DSL-FIQA AND TOPIQ-SWIN HIGHLIGHT OUR FRAMEWORK'S CAPACITY TO MAINTAIN FACIAL STRUCTURAL INTEGRITY ACROSS DIFFERENT AGE GROUPS. **RED** AND **BLUE** INDICATE BEST AND SECOND-BEST RESULTS.

CelebChild-Test Methods	Natural Image Quality Evaluation				Face Image Quality Evaluation		
	FID↓	MUSIQ↑	CLIPQA+↑	MANIQA↑	topiq↑	topiq-swin↑	DSL-FIQA↑
GFPGAN	120.9049	74.1155	0.6166	0.5345	0.7484	0.7917	0.8419
GPEN	109.1407	70.3653	0.5491	0.4307	0.6393	0.7341	0.7429
DR2	137.0317	69.6723	0.6025	0.4982	0.6918	0.7776	0.8063
DifFace	106.2445	66.6574	0.5285	0.4206	0.5935	0.7021	0.7079
RestoreFormer	102.8651	70.5183	0.5708	0.5425	0.6840	0.7474	0.7921
DAEFR	108.2202	73.7093	0.6240	0.5141	0.7189	0.7961	0.8154
Codeformer	124.3481	73.6569	0.6171	0.4985	0.7342	0.8020	0.8279
VQFR	117.9200	72.3455	0.5962	0.5073	0.7090	0.7819	0.8154
Pref-Restore	105.9776	76.0753	0.7016	0.5727	0.8121	0.8744	0.8859

including GAN-based models (GPGGAN [1], GPEN [2]) and Codebook-based priors (DAEFR [7], CodeFormer [4]).

Fidelity vs. Quality Trade-off. A defining characteristic of our framework is the distinct functional roles of its two variants: *Pref-Restore Fidelity* which prioritizes structural fidelity, and *Pref-Restore Quality*³ which optimizes for perceptual quality through preference-aligned fine-tuning. This dual-variant approach allows for a flexible balance between reconstruction accuracy and aesthetic realism.

As illustrated in Fig. 4, *Pref-Restore (F)* exhibits superior structural consistency with the ground truth, particularly in recovering intricate identity-defining features. In the first and third rows, the model precisely restores complex details such as the specific frames of eyeglasses and the nuanced gaze of the eyes—elements that are frequently distorted or omitted by baselines like GPEN or DR2. This performance validates that our *Texture-to-Diffusion Alignment* effectively anchors the diffusion process to the original facial manifold, preventing identity drift even under severe degradation.

Building upon this structural foundation, *Pref-Restore (Q)* further refines the output to align with human visual preferences. While preserving the core structural integrity established in stage 1, the (Q) variant produces significantly more vivid textures and sharper facial contours. For example, in the second row (depicting blonde hair), where CodeFormer tends to yield over-smoothed or plastic-like skin textures, our (Q) model restores natural pore-level details and lifelike hair strands. This enhancement demonstrates the efficacy of the DiffusionNFT mechanism in regularizing the generative field to suppress artifacts and prioritize high-fidelity, perceptually rich textures.

Comparison with Baselines. Traditional GAN-based methods (GPGGAN, GPEN) frequently suffer from identity drifting or unnatural light artifacts when handling severe blur. While codebook-based methods like CodeFormer and VQFR improve robustness, they often struggle to reconstruct intricate high-frequency details, particularly in hair regions. As shown in the second and fourth rows of Fig. 4, CodeFormer and VQFR tend to produce over-smoothed or blurred hair textures, failing to capture the lifelike strands present in the ground truth. In contrast, our *Pref-Restore* variants, benefited by the *Texture-to-Diffusion Alignment*, successfully preserve the grain and flow of the hair, delivering results that are both perceptually sharper and more faithful to the original distribution.

D. The Role of Multi-modal Text Guidance

While conventional restoration metrics often focus on low-level pixel alignment or general perceptual quality, they frequently fail to capture the *semantic fidelity* of the reconstructed content. To investigate the impact of multi-modal text guidance on semantic-level restoration, we conduct a controlled comparative study.

Experimental Setup. We utilize the Qwen2.5VL-32B [69] model to generate detailed descriptive captions for each image

³For brevity, we refer to these variants as *Pref-Restore (F)* and *Pref-Restore (Q)*, respectively, in the remainder of this paper.

TABLE VII
QUANTITATIVE IMPACT OF TEXT GUIDANCE ON SEMANTIC RESTORATION. THE METRICS FOCUS ON HIGH-LEVEL FEATURE SIMILARITY AND PERCEPTUAL CONSISTENCY RATHER THAN PIXEL-LEVEL NOISE REDUCTION. +CAPTION DENOTES THE MODEL TRAINED WITH DETAILED QWEN2.5VL-GENERATED DESCRIPTIONS.

Metric	Base model	+Caption	Improvement (\uparrow)
ClipScore-I \uparrow	0.7435	0.8193	+0.0758
ClipScore-T \uparrow	0.2610	0.2631	+0.0021
DreamSim \uparrow	0.7405	0.8026	+0.0621

in our training dataset. We then compare two training configurations:

- *Base Model*: Trained with a generic instruction: "<image>\nPlease reconstruct the given image."
- *Caption-augmented Model (+Caption)*: Trained with content-aware instructions: "<image>\nPlease reconstruct the given image based on the image content: {prompt}", where {prompt} is the detailed caption generated by Qwen2.5VL.

All other architectural components and training hyperparameters remain identical between the two groups.

Semantic Evaluation Metrics. Since the primary objective of text guidance is to enhance high-level semantic consistency rather than pixel-wise accuracy, we employ three specialized metrics for evaluation:

- *ClipScore-I* [70]: Measures the latent feature similarity between the restored image and the ground truth image using the CLIP vision backbone.
- *ClipScore-T* [70]: Assesses the alignment between the restored image and the reference text description.
- *DreamSim* [71]: A state-of-the-art perceptual metric that focuses on mid-to-high level semantic similarity, better aligning with human judgment of "content consistency."

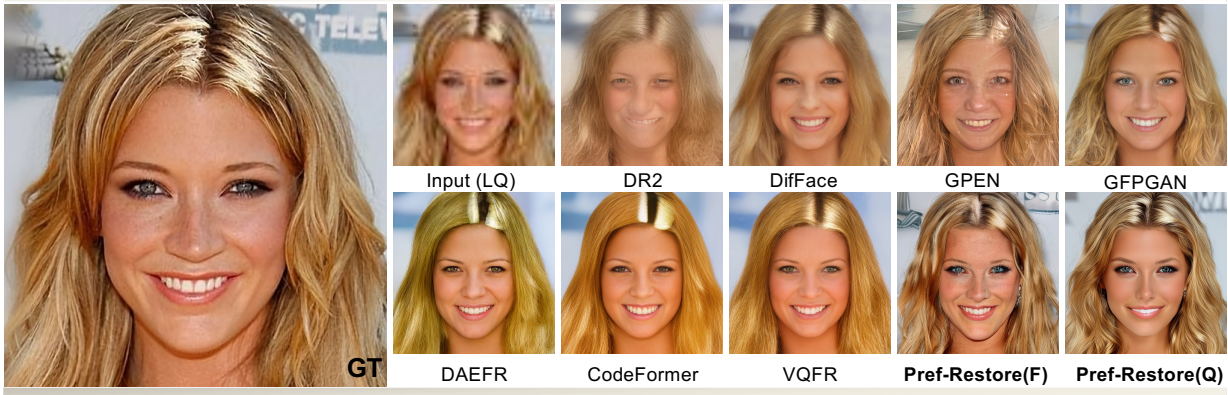
Quantitative Analysis. The results, summarized in Table VII, reveal that incorporating text guidance leads to substantial improvements in semantic-level restoration. Specifically, *ClipScore-I* increases from 0.7435 to 0.8193 (+10.2%), and *DreamSim* improves from 0.7405 to 0.8026 (+8.4%).

The significant gain in *ClipScore-I* and *DreamSim* indicates that text guidance provides a strong structural and semantic prior, enabling the Auto-Regressive module to better bridge the information gap in severely degraded regions. Although the improvement in *ClipScore-T* is relatively modest (0.2610 to 0.2631), the overall trend confirms that the model is successfully utilizing the text tokens to anchor the generative process towards more plausible and content-consistent manifolds. This empirical evidence supports our hypothesis that multi-modal instructions are crucial for solving the ill-posed nature of blind face restoration at a semantic level.

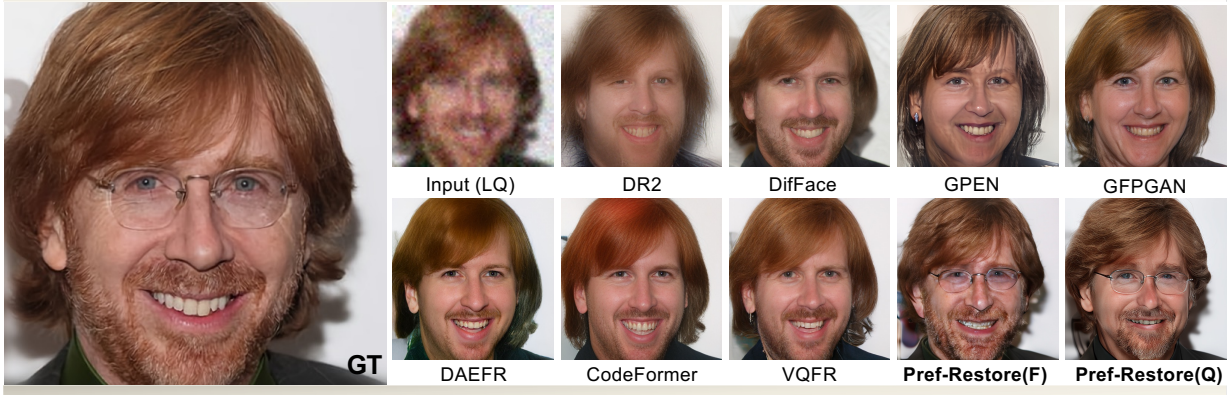
Qualitative Analysis. To provide a more intuitive understanding, we visualize the restoration outcomes (Fig. 5). The comparison highlights the vulnerability of pure visual restoration models when facing extreme degradation. As shown in the second row, the baseline model (*w.o. text*), lacking sufficient



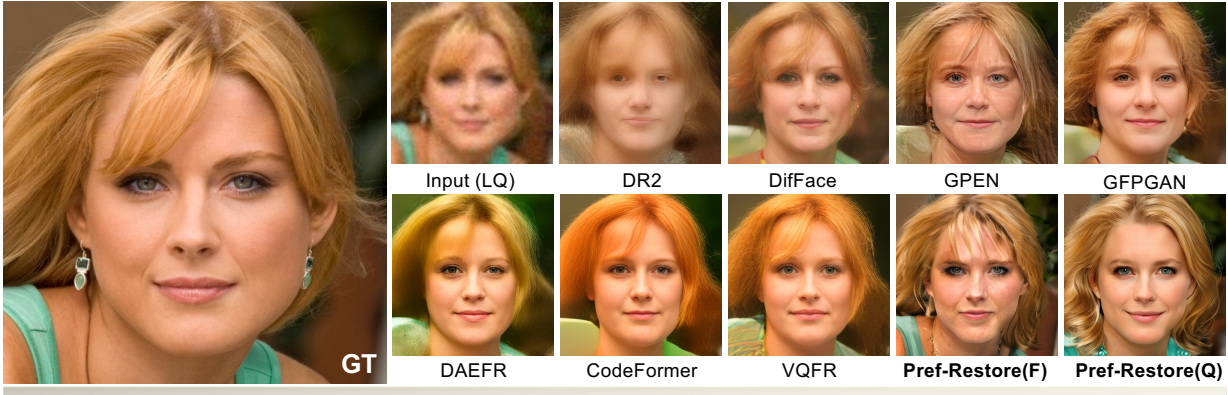
Caption: A photography of a person with wavy brown hair and a large, elegant white hat.



Caption: A photograph of a person with long, wavy blonde hair, standing against a backdrop with text.



Caption: A photography of a person with medium-length, light brown hair wearing a black blazer against a white background.



Caption: A photography of a person with blonde hair, wearing a turquoise top and silver hoop earrings.

Fig. 4. **Qualitative comparison of face restoration on the CelebA-HQ dataset.** We compare our **Pref-Restore (F)** and **(Q)** variants with state-of-the-art methods. Our models demonstrate superior performance in recovering structural details and high-frequency hair textures compared to baselines like CodeFormer and VQFR, which often suffer from over-smoothing in complex regions. The **(Q)** variant further enhances aesthetic clarity and texture realism through preference-aware RL optimization.

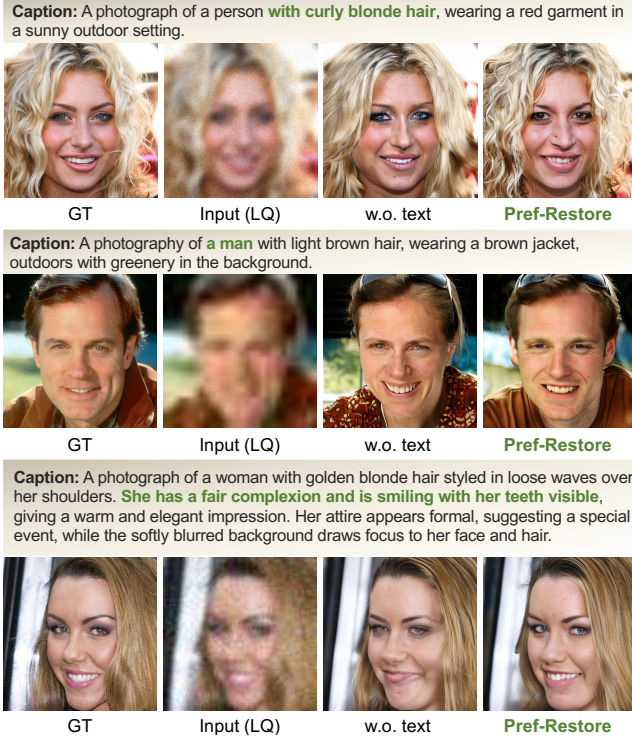


Fig. 5. **Visual comparison illustrating the impact of multi-modal text guidance.** We present three cases where the degradation is severe. Without text guidance (*w.o. text*), the model relies solely on the ambiguous visual priors, leading to critical semantic failures: (Top) Misinterpreting “curly blonde hair” as straight hair; (Middle) Hallucinating a female face for a male subject (Identity Error); (Bottom) Losing the “smiling with teeth visible” attribute.

identity cues from the severely blurred input, incorrectly reconstructs a female face from a male subject, resulting in a catastrophic identity shift. Similarly, in the first and third rows, fine-grained attributes such as “curly hair” and “smiling with teeth” are lost or smoothed out. However, by injecting explicit semantic tokens (e.g., “a man”, “curly blonde hair”, “teeth visible”), our *Pref-Restore* effectively utilizes text as a semantic anchor. This enables the model to break the symmetry of ill-posed solutions and deterministically recover the correct attributes, verifying that text guidance serves as a critical disambiguation signal in the latent space.

The convergence of both quantitative gains and qualitative fidelity strongly supports our hypothesis: multi-modal instructions are indispensable for solving the information sparsity in blind face restoration.

E. Preference-Aware Fine-tuning via DiffusionNFT

To further bridge the gap between deterministic reconstruction and high-quality human visual preferences, we analyze the impact of Stage 2: Preference-Aware Fine-tuning via DiffusionNFT. This stage aims to refine the generative vector field by optimizing a compound reward function that encapsulates aesthetic appeal, semantic consistency, and human choice priors.

Reward Composition and Quantitative Gains. Our preference reward $\mathcal{R}_{\text{pref}}$ is a synergistic ensemble of three state-of-the-art multi-modal scoring models: *HPSv2* [72] (Human Preference Score), *Clip Score* [73] (Semantic alignment), and

TABLE VIII
QUANTITATIVE COMPARISON OF PREFERENCE METRICS BEFORE AND AFTER DIFFUSIONNFT FINE-TUNING. THE SIGNIFICANT GAINS IN *HPSv2* AND *PICK SCORE* INDICATE A SUBSTANTIAL IMPROVEMENT IN AESTHETIC QUALITY AND ALIGNMENT WITH HUMAN VISUAL PREFERENCES.

Model Variant	<i>HPSv2</i> \uparrow	Clip Score \uparrow	Pick Score \uparrow
PrefRestore-Base (Stage 1)	22.28	19.67	20.01
PrefRestore-RL (Stage 2)	30.22	21.10	22.53

Stage 2: Preference-Aware Optimization Dynamics

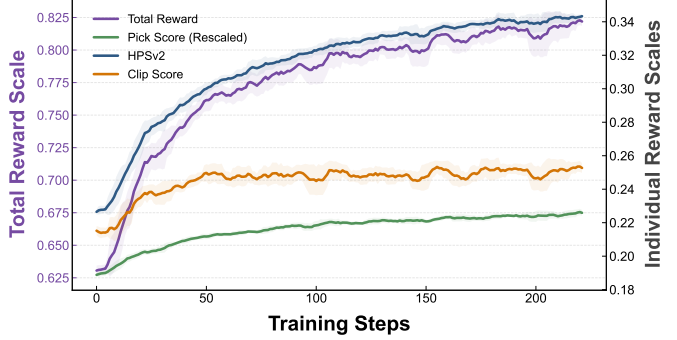


Fig. 6. **Evolution of preference-aware rewards during DiffusionNFT fine-tuning.** We employ a dual-axis visualization to demonstrate the synchronized optimization of diverse metrics. The *Total Reward* (purple line, left axis) represents the aggregate alignment, while *HPSv2*, *Clip Score*, and *Pick Score* occupy the right axis to reflect fine-grained preference gains. The stable growth across all components validates the robustness of our on-policy RL optimization in refining the generative manifold.

Pick Score [74] (General aesthetic and quality prior). As summarized in Table VIII, comparing the *PrefRestore-Base* (end of Stage 1) with the *PrefRestore-RL* (end of Stage 2) reveals substantial improvements across all preference-related dimensions. Notably, the *HPSv2* increases significantly from 22.28 to 30.22 (+35.6%), and the *Pick Score* rises from 76.98 to 86.66 (+12.6%). These gains empirically demonstrate that the DiffusionNFT mechanism successfully rotates the velocity field towards the manifold preferred by human observers, enhancing the overall visual pleasantness of the restored faces.

Optimization Dynamics. To further investigate the stability and effectiveness of the preference-aware fine-tuning, we monitor the evolution of both aggregate and individual reward components throughout Stage 2. As illustrated in Fig. 6, we employ a dual-axis visualization to accommodate the varying scales of different reward models. The *Total Reward* (purple line, left axis) is formulated as the summation of *HPSv2*, *Clip Score*, and *Pick Score*.

A pivotal observation is that all metrics exhibit a sustained and synchronized upward trajectory. Specifically, the sharp initial rise in *HPSv2* and *Total Reward* suggests that the Forward Flow Contrast objective in DiffusionNFT provides a robust gradient signal, allowing the model to rapidly identify and reinforce the high-fidelity generative manifold preferred by human observers. This stable optimization process underscores the superiority of our DiffusionNFT framework in aligning large-scale generative models with sophisticated perceptual priors.

TABLE IX
ABLATION STUDY OF STAGE 1.2 (TEXTURE-TO-DIFFUSION ALIGNMENT). THE METRICS ARE CALCULATED ON THE VALIDATION SET. *Stage 1.1 + 1.2* DENOTES OUR FULL MODEL AFTER STAGE 1. LOWER VALUES INDICATE BETTER PERFORMANCE FOR ALL LISTED METRICS.

Configuration	LPIPS ↓	FID ↓	LMD ↓	Deg ↓
Stage 1.1 only	0.5272	23.2199	8.6819	74.5286
Stage 1.1 + 1.2	0.4175	16.2435	5.1337	54.0623

F. Ablation Study: Texture-to-Diffusion Alignment

To verify the necessity of the two-step strategy in our Stage 1 training, we conduct an ablation study focusing on the *Texture-to-Diffusion Alignment*. While the initial *Semantic-to-Diffusion Alignment* successfully bridges the modality gap between the AR-generated semantic tokens and the Diffusion latent space, it often struggles to recover high-frequency textures due to the information bottleneck in compressed latent representations.

Experimental Setup. We compare the performance of the following two configurations:

- *Stage 1.1 Only*: The model is trained solely using the semantic alignment loss, where the Diffusion module reconstructs the image based only on the AR output and degraded input.
- *Stage 1.1 + Stage 1.2 (Full)*: The complete Stage 1 model, which incorporates the Texture-aware Feature Refinement module to inject multi-scale, fine-grained visual cues from the VAE encoder into the generative process.

Quantitative Analysis. As shown in Table IX, the integration of Step 2 leads to a remarkable improvement across all reference-based fidelity metrics. Specifically, the *LPIPS* decreases from 0.5272 to 0.4175, indicating a significant boost in perceptual similarity to the ground truth. The *FID (HQ)* drops from 23.2199 to 16.2435 (a 30.0% improvement).

Furthermore, we observe a substantial reduction in the *LMD* from 8.6819 to 5.1337 and the *Deg* from 74.5286 to 54.0623. These results suggest that the texture-aware refinement not only restores pixel-level details but also significantly enhances the *structural fidelity* and *identity consistency* of the reconstructed faces. The fine-grained features act as a crucial anchor, preventing the generative model from producing plausible but identity-drifting hallucinations. This evidence justifies the design of our hierarchical training strategy in Stage 1.

G. Trade-off between Fidelity and Aesthetic Quality

A unique characteristic of our framework is the coexistence of two specialized variants: *Pref-Restore(F)* (Fidelity-oriented) and *Pref-Restore(Q)* (Quality-oriented). While the Stage 2 RL fine-tuning significantly elevates the aesthetic appeal, it inherently introduces a trade-off between perceived quality and pixel-level fidelity. As illustrated in Fig. 7, we categorize the restoration outcomes into two distinct scenarios to further dissect this dynamic.

Scenario 1: Over-refinement and Fidelity Loss. In certain cases, as shown in the top two rows (Fig. 7 (a)), the powerful generative prior of *Pref-Restore(Q)* leads to “over-beautification”. While the RL-tuned model produces excep-

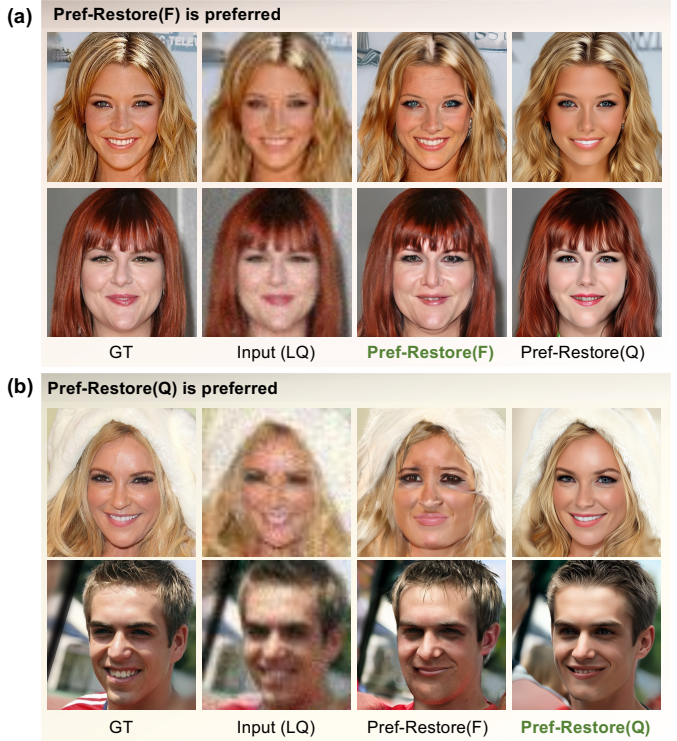


Fig. 7. Qualitative comparison between *Pref-Restore(F)* and *Pref-Restore(Q)*. (a): Situations where *Pref-Restore(F)* is preferred for its superior preservation of original identity details, whereas the (Q) variant exhibits slight over-beautification. (b): Cases where *Pref-Restore(Q)* is preferred, as the RL-based fine-tuning effectively rectifies unnatural artifacts and perceptual inconsistencies produced in Stage 1.

tionally smooth skin textures and idealized facial symmetry, it occasionally suppresses subtle but critical identity markers present in the original image. For instance, tiny beauty marks, specific wrinkle patterns, or nuanced structural asymmetries that are faithfully preserved by *Pref-Restore(F)* might be regularized in the (Q) variant to satisfy high-reward aesthetic priors. This highlights that for applications requiring strict forensic-level identity preservation, the Stage 1 output (*Pref-Restore(F)*) remains the more reliable choice.

Scenario 2: Preference-aware Error Correction. Conversely, the bottom two rows (Fig. 7 (b)) demonstrate the restorative power of RL alignment. In these instances, *Pref-Restore(F)* might suffer from “hallucination artifacts” or unnatural facial expressions due to the inherent stochasticity of the diffusion base. The RL process, guided by human preference models (HPSv2 and PickScore), successfully identifies these perceptual “glitches” and steers the denoising trajectory towards a more natural and plausible manifold. The (Q) variant effectively corrects the distorted gaze or awkward mouth shapes found in the (F) version, resulting in a face that is not only more aesthetically pleasing but also more perceptually coherent.

This dual-variant strategy allows users to dynamically adjust the restoration focus depending on the downstream task to prioritize either the veracity of Stage 1 or the perceptual perfection of Stage 2.

H. Bridging Information Asymmetry: Deterministic Analysis

The inherent ill-posedness of blind face restoration often leads to a significant *information asymmetry* between the degraded input and the high-fidelity output. Stochastic generative models, while capable of producing high-quality textures, frequently suffer from a vast and unconstrained solution space, resulting in inconsistent hallucinations across different sampling runs.

To demonstrate how our hierarchical framework bridges this information asymmetry and enforces a more deterministic restoration, we conduct a rigorous stability analysis. As illustrated in Fig. 8, we compare the *Base Model* with our *Pref-Restore* by performing $N = 16$ independent restoration runs for each test image under different random seeds. We calculate the standard deviation of various perceptual metrics, including HPSv2, PickScore, ClipScore, and their Sum Score, to quantify the sampling variance.

Quantitative Variance Reduction. To verify the impact of our framework on mitigating restoration uncertainty, we conduct a statistical analysis of score fluctuations across multiple preference dimensions. As illustrated in the boxplots (a-d) of Fig. 8, *Pref-Restore* exhibits a substantial reduction in variance compared to the base generative model. Specifically, the median standard deviation of the *Sum Score* drops significantly from approximately 0.032 to 0.016, representing a 50% reduction in restoration stochasticity.

This trend of enhanced stability persists even in complex semantic metrics such as *HPSv2* and *PickScore*. The significantly tighter interquartile ranges and more concentrated distributions indicate that our hierarchical constraints—which synergize AR-based semantic alignment with RL-refined aesthetic priors—effectively anchor the diffusion denoising trajectory. By narrowing the solution space, the framework ensures that the generative process no longer oscillates between disparate interpretations of the same degraded input, but instead converges toward a consistent, high-preference output.

Conclusion on Deterministic Restoration. These results provide empirical evidence that our framework successfully narrows the solution space. By injecting fine-grained visual cues and human-aligned preference priors, we bridge the gap between stochastic generation and deterministic restoration. This ensures that the model produces not just “a plausible face,” but the *most likely and consistent* reconstruction, fulfilling the requirements of deterministic blind face restoration.

VI. CONCLUSION

In this paper, we propose *Pref-Restore*, a novel hierarchical framework that effectively bridges the information asymmetry inherent in blind face restoration to achieve deterministic and high-fidelity results. By synergizing a two-step alignment strategy in Stage 1 — comprising Semantic-to-Diffusion Alignment and Texture-aware Feature Refinement — with a preference-aware reinforcement learning paradigm in Stage 2, our method successfully anchors the generative process to a stable facial manifold while suppressing unnatural artifacts. Experimental results and stability analysis demonstrate that *Pref-Restore* not only outperforms state-of-the-art methods in

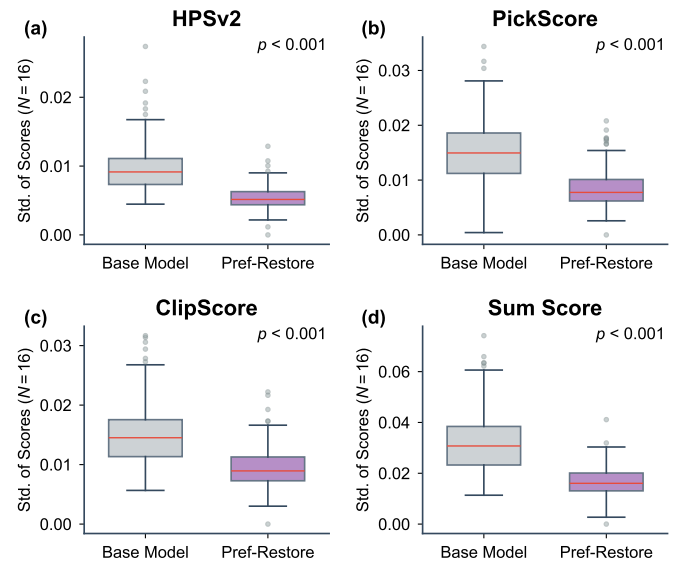


Fig. 8. **Quantitative analysis of solution space reduction.** We report the standard deviation of scores across $N = 16$ independent sampling runs for (a) HPSv2, (b) PickScore, (c) ClipScore, and (d) the aggregate Sum Score. Compared to the Base Model, our *Pref-Restore* consistently achieves significantly lower variance and a tighter distribution. This validates that our hierarchical framework effectively constrains the stochastic sampling process, leading to a more stable and deterministic restoration performance.

restoring intricate high-frequency textures but also significantly narrows the solution space, yielding a 50% reduction in sampling variance. The flexibility offered by our dual-variant strategy (Fidelity vs. Quality) underscores the potential of our framework for diverse real-world applications, and future work will extend this hierarchical preference-aware logic to more complex video-based and general generative tasks.

REFERENCES

- [1] X. Wang, Y. Li, H. Zhang, and Y. Shan, “Towards real-world blind face restoration with generative facial prior,” in *Proceedings of the IEEE/CVF conference on computer vision and pattern recognition*, 2021, pp. 9168–9178.
- [2] T. Yang, P. Ren, X. Xie, and L. Zhang, “Gan prior embedded network for blind face restoration in the wild,” in *Proceedings of the IEEE/CVF conference on computer vision and pattern recognition*, 2021, pp. 672–681.
- [3] Y. Gu, X. Wang, L. Xie, C. Dong, G. Li, Y. Shan, and M.-M. Cheng, “Vqfr: Blind face restoration with vector-quantized dictionary and parallel decoder,” in *European Conference on Computer Vision*. Springer, 2022, pp. 126–143.
- [4] S. Zhou, K. Chan, C. Li, and C. C. Loy, “Towards robust blind face restoration with codebook lookup transformer,” *Advances in Neural Information Processing Systems*, vol. 35, pp. 30599–30611, 2022.
- [5] Z. Yue and C. C. Loy, “Difface: Blind face restoration with diffused error contraction,” *IEEE Transactions on Pattern Analysis and Machine Intelligence*, 2024.
- [6] Z. Wang, Z. Zhang, X. Zhang, H. Zheng, M. Zhou, Y. Zhang, and Y. Wang, “Dr2: Diffusion-based robust degradation remover for blind face restoration,” in *Proceedings of the IEEE/CVF Conference on Computer Vision and Pattern Recognition*, 2023, pp. 1704–1713.
- [7] Y.-J. Tsai, Y.-L. Liu, L. Qi, K. C. Chan, and M.-H. Yang, “Dual associated encoder for face restoration,” *arXiv preprint arXiv:2308.07314*, 2023.
- [8] Y.-L. You and M. Kaveh, “Blind image restoration by anisotropic regularization,” *IEEE Transactions on Image Processing*, vol. 8, no. 3, pp. 396–407, 1999.

[9] D. Kundur and D. Hatzinakos, "Blind image deconvolution," *IEEE signal processing magazine*, vol. 13, no. 3, pp. 43–64, 2002.

[10] Z. Yue, H. Yong, Q. Zhao, L. Zhang, D. Meng, and K.-Y. K. Wong, "Deep variational network toward blind image restoration," *IEEE Transactions on Pattern Analysis and Machine Intelligence*, vol. 46, no. 11, pp. 7011–7026, 2024.

[11] X. Lin, J. He, Z. Chen, Z. Lyu, B. Dai, F. Yu, W. Ouyang, Y. Qiao, and C. Dong, "Diffbir: Towards blind image restoration with generative diffusion prior," *arXiv preprint arXiv:2308.15070*, 2023.

[12] J. Hu, Z. Yao, L. Jin, Y. Chen, and Y. Lu, "Universal image restoration pre-training via masked degradation classification," *arXiv preprint arXiv:2510.13282*, 2025.

[13] J. Jiang, Z. Zuo, G. Wu, K. Jiang, and X. Liu, "A survey on all-in-one image restoration: Taxonomy, evaluation and future trends," *IEEE Transactions on Pattern Analysis and Machine Intelligence*, 2025.

[14] C. Ledig, L. Theis, F. Huszár, J. Caballero, A. Cunningham, A. Acosta, A. Aitken, A. Tejani, J. Totz, Z. Wang *et al.*, "Photo-realistic single image super-resolution using a generative adversarial network," in *Proceedings of the IEEE conference on computer vision and pattern recognition*, 2017, pp. 4681–4690.

[15] X. Wang, K. Yu, S. Wu, J. Gu, Y. Liu, C. Dong, Y. Qiao, and C. Change Loy, "EsrGAN: Enhanced super-resolution generative adversarial networks," in *Proceedings of the European conference on computer vision (ECCV) workshops*, 2018, pp. 0–0.

[16] X. Ji, Y. Cao, Y. Tai, C. Wang, J. Li, and F. Huang, "Real-world super-resolution via kernel estimation and noise injection," in *proceedings of the IEEE/CVF conference on computer vision and pattern recognition workshops*, 2020, pp. 466–467.

[17] D. P. Kingma and M. Welling, "Auto-encoding variational bayes," *arXiv preprint arXiv:1312.6114*, 2013.

[18] I. Goodfellow, J. Pouget-Abadie, M. Mirza, B. Xu, D. Warde-Farley, S. Ozair, A. Courville, and Y. Bengio, "Generative adversarial nets," *Advances in neural information processing systems*, vol. 27, 2014.

[19] J. Ho, A. Jain, and P. Abbeel, "Denoising diffusion probabilistic models," *Advances in neural information processing systems*, vol. 33, pp. 6840–6851, 2020.

[20] Y. Song and S. Ermon, "Generative modeling by estimating gradients of the data distribution," *Advances in neural information processing systems*, vol. 32, 2019.

[21] X. Pan, S. N. Shukla, A. Singh, Z. Zhao, S. K. Mishra, J. Wang, Z. Xu, J. Chen, K. Li, F. Juefei-Xu *et al.*, "Transfer between modalities with metaqueries," *arXiv preprint arXiv:2504.06256*, 2025.

[22] J. Chen, L. Xue, Z. Xu, X. Pan, S. Yang, C. Qin, A. Yan, H. Zhou, Z. Chen, L. Huang *et al.*, "Blip3o-next: Next frontier of native image generation," *arXiv preprint arXiv:2510.15857*, 2025.

[23] J. Han, H. Chen, Y. Zhao, H. Wang, Q. Zhao, Z. Yang, H. He, X. Yue, and L. Jiang, "Vision as a dialect: Unifying visual understanding and generation via text-aligned representations," *arXiv preprint arXiv:2506.18898*, 2025.

[24] J. Hu, Y. Yang, J. Liu, J. Wu, C. Zhao, and Y. Lu, "Auto-regressively generating multi-view consistent images," *arXiv preprint arXiv:2506.18527*, 2025.

[25] J. Hu, S. Zhao, Q.-G. Chen, X. Qiu, J. Liu, Z. Xu, W. Luo, K. Zhang, and Y. Lu, "Omni-view: Unlocking how generation facilitates understanding in unified 3d model based on multiview images," *arXiv preprint arXiv:2511.07222*, 2025.

[26] B. Lin, Z. Li, X. Cheng, Y. Niu, Y. Ye, X. He, S. Yuan, W. Yu, S. Wang, Y. Ge *et al.*, "Uniworld: High-resolution semantic encoders for unified visual understanding and generation," *arXiv preprint arXiv:2506.03147*, 2025.

[27] Z. Shao, P. Wang, Q. Zhu, R. Xu, J. Song, X. Bi, H. Zhang, M. Zhang, Y. Li, Y. Wu *et al.*, "Deepseekmath: Pushing the limits of mathematical reasoning in open language models," *arXiv preprint arXiv:2402.03300*, 2024.

[28] J. Liu, G. Liu, J. Liang, Y. Li, J. Liu, X. Wang, P. Wan, D. Zhang, and W. Ouyang, "Flow-grpo: Training flow matching models via online rl," *arXiv preprint arXiv:2505.05470*, 2025.

[29] K. Zheng, H. Chen, H. Ye, H. Wang, Q. Zhang, K. Jiang, H. Su, S. Ermon, J. Zhu, and M.-Y. Liu, "Diffusionnft: Online diffusion reinforcement with forward process," *arXiv preprint arXiv:2509.16117*, 2025.

[30] Y. Chen, Y. Tai, X. Liu, C. Shen, and J. Yang, "Fsrnet: End-to-end learning face super-resolution with facial priors," in *Proceedings of the IEEE conference on computer vision and pattern recognition*, 2018, pp. 2492–2501.

[31] C. Chen, X. Li, L. Yang, X. Lin, L. Zhang, and K.-Y. K. Wong, "Progressive semantic-aware style transformation for blind face restoration," in *Proceedings of the IEEE/CVF conference on computer vision and pattern recognition*, 2021, pp. 11896–11905.

[32] X. Hu, W. Ren, J. LaMaster, X. Cao, X. Li, Z. Li, B. Menze, and W. Liu, "Face super-resolution guided by 3d facial priors," in *Computer Vision–ECCV 2020: 16th European Conference, Glasgow, UK, August 23–28, 2020, Proceedings, Part IV 16*. Springer, 2020, pp. 763–780.

[33] B. Dogan, S. Gu, and R. Timofte, "Exemplar guided face image super-resolution without facial landmarks," in *Proceedings of the IEEE/CVF conference on computer vision and pattern recognition workshops*, 2019, pp. 0–0.

[34] X. Li, C. Chen, S. Zhou, X. Lin, W. Zuo, and L. Zhang, "Blind face restoration via deep multi-scale component dictionaries," in *European conference on computer vision*. Springer, 2020, pp. 399–415.

[35] T. Karras, S. Laine, and T. Aila, "A style-based generator architecture for generative adversarial networks," in *Proceedings of the IEEE/CVF conference on computer vision and pattern recognition*, 2019, pp. 4401–4410.

[36] J. Gu, Y. Shen, and B. Zhou, "Image processing using multi-code gan prior," in *Proceedings of the IEEE/CVF conference on computer vision and pattern recognition*, 2020, pp. 3012–3021.

[37] S. Menon, A. Damian, S. Hu, N. Ravi, and C. Rudin, "Pulse: Self-supervised photo upsampling via latent space exploration of generative models," in *Proceedings of the ieee/cvf conference on computer vision and pattern recognition*, 2020, pp. 2437–2445.

[38] H. Wei, S. Liu, C. Yuan, and L. Zhang, "Perceive, understand and restore: Real-world image super-resolution with autoregressive multimodal generative models," *arXiv preprint arXiv:2503.11073*, 2025.

[39] A. Radford, J. W. Kim, C. Hallacy, A. Ramesh, G. Goh, S. Agarwal, G. Sastry, A. Askell, P. Mishkin, J. Clark *et al.*, "Learning transferable visual models from natural language supervision," in *International conference on machine learning*. PMLR, 2021, pp. 8748–8763.

[40] V. Potlapalli, S. W. Zamir, S. H. Khan, and F. Shahbaz Khan, "Promptir: Prompting for all-in-one image restoration," *Advances in Neural Information Processing Systems*, vol. 36, pp. 71275–71293, 2023.

[41] M. V. Conde, G. Geigle, and R. Timofte, "Instructir: High-quality image restoration following human instructions," in *European Conference on Computer Vision*. Springer, 2024, pp. 1–21.

[42] Z. Luo, F. K. Gustafsson, Z. Zhao, J. Sjölund, and T. B. Schön, "Controlling vision-language models for multi-task image restoration," *arXiv preprint arXiv:2310.01018*, 2023.

[43] K. Yu, C. Dong, L. Lin, and C. C. Loy, "Crafting a toolchain for image restoration by deep reinforcement learning," in *Proceedings of IEEE Conference on Computer Vision and Pattern Recognition*, 2018, pp. 2443–2452.

[44] K. Yu, X. Wang, C. Dong, X. Tang, and C. C. Loy, "Path-restore: Learning network path selection for image restoration," *IEEE Transactions on Pattern Analysis and Machine Intelligence*, 2021.

[45] L. Ouyang, J. Wu, X. Jiang, D. Almeida, C. Wainwright, P. Mishkin, C. Zhang, S. Agarwal, K. Slama, A. Ray *et al.*, "Training language models to follow instructions with human feedback," *Advances in neural information processing systems*, vol. 35, pp. 27730–27744, 2022.

[46] B. Wu, W. Wang, Y. Liu, Z. Li, and Y. Zhao, "Diffusionreward: Enhancing blind face restoration through reward feedback learning," *arXiv preprint arXiv:2505.17910*, 2025.

[47] R. Rafailov, A. Sharma, E. Mitchell, C. D. Manning, S. Ermon, and C. Finn, "Direct preference optimization: Your language model is secretly a reward model," *Advances in neural information processing systems*, vol. 36, pp. 53728–53741, 2023.

[48] M. Cai, S. Li, W. Li, X. Huang, H. Chen, J. Hu, and Y. Wang, "Dspo: Direct semantic preference optimization for real-world image super-resolution," *arXiv preprint arXiv:2504.15176*, 2025.

[49] H. X. Y. Liu, B. Jiang, J. Peng, D. Luo, X. Hu, S. Yan, and H. Li, "Irpo: Boosting image restoration via post-training grpo," *arXiv preprint arXiv:2512.00814*, 2025.

[50] J. Qiao, M. Cai, W. Li, Y. Liu, X. Huang, G. He, J. Xie, J. Hu, X. Chen, and S. Lin, "Realusr-r1: Reinforcement learning for real-world image super-resolution with vision-language chain-of-thought," *arXiv preprint arXiv:2506.16796*, 2025.

[51] B. Li, X. Li, J. Xu, J. Guo, W. Li, R. Pei, and Z. Chen, "Test-time preference optimization for image restoration," *arXiv preprint arXiv:2511.19169*, 2025.

[52] H. Chen, K. Zheng, Q. Zhang, G. Cui, Y. Cui, H. Ye, T.-Y. Lin, M.-Y. Liu, J. Zhu, and H. Wang, "Bridging supervised learning and reinforcement learning in math reasoning," *arXiv preprint arXiv:2505.18116*, 2025.

[53] C. E. Shannon, "A mathematical theory of communication," *The Bell System Technical Journal*, vol. 27, no. 3, pp. 379–423, 1948.

[54] Y. LeCun, S. Chopra, R. Hadsell, M. Ranzato, and F. Huang, “A tutorial on energy-based learning,” *Predicting structured data*, vol. 1, no. 0, 2006.

[55] M. Tschannen, A. Gritsenko, X. Wang, M. F. Naeem, I. Alabdulmohsin, N. Parthasarathy, T. Evans, L. Beyer, Y. Xia, B. Mustafa *et al.*, “Siglip 2: Multilingual vision-language encoders with improved semantic understanding, localization, and dense features,” *arXiv preprint arXiv:2502.14786*, 2025.

[56] E. Xie, J. Chen, Y. Zhao, J. Yu, L. Zhu, C. Wu, Y. Lin, Z. Zhang, M. Li, J. Chen *et al.*, “Sana 1.5: Efficient scaling of training-time and inference-time compute in linear diffusion transformer,” *arXiv preprint arXiv:2501.18427*, 2025.

[57] T. Karras, S. Laine, and T. Aila, “A style-based generator architecture for generative adversarial networks,” in *Proceedings of the IEEE/CVF conference on computer vision and pattern recognition*, 2019, pp. 4401–4410.

[58] T. Karras, “Progressive growing of gans for improved quality, stability, and variation,” *arXiv preprint arXiv:1710.10196*, 2017.

[59] G. B. Huang, M. Mattar, T. Berg, and E. Learned-Miller, “Labeled faces in the wild: A database for studying face recognition in unconstrained environments,” in *Workshop on faces in 'Real-Life' Images: detection, alignment, and recognition*, 2008.

[60] S. Yang, P. Luo, C.-C. Loy, and X. Tang, “Wider face: A face detection benchmark,” in *Proceedings of the IEEE conference on computer vision and pattern recognition*, 2016, pp. 5525–5533.

[61] R. Zhang, P. Isola, A. A. Efros, E. Shechtman, and O. Wang, “The unreasonable effectiveness of deep features as a perceptual metric,” in *Proceedings of the IEEE conference on computer vision and pattern recognition*, 2018, pp. 586–595.

[62] M. Heusel, H. Ramsauer, T. Unterthiner, B. Nessler, and S. Hochreiter, “Gans trained by a two time-scale update rule converge to a local nash equilibrium,” *Advances in neural information processing systems*, vol. 30, 2017.

[63] J. Ke, Q. Wang, Y. Wang, P. Milanfar, and F. Yang, “Musiq: Multi-scale image quality transformer,” in *Proceedings of the IEEE/CVF international conference on computer vision*, 2021, pp. 5148–5157.

[64] J. Wang, K. C. Chan, and C. C. Loy, “Exploring clip for assessing the look and feel of images,” in *Proceedings of the AAAI Conference on Artificial Intelligence*, vol. 37, no. 2, 2023, pp. 2555–2563.

[65] S. Yang, T. Wu, S. Shi, S. Lao, Y. Gong, M. Cao, J. Wang, and Y. Yang, “Maniq: Multi-dimension attention network for no-reference image quality assessment,” in *Proceedings of the IEEE/CVF Conference on Computer Vision and Pattern Recognition*, 2022, pp. 1191–1200.

[66] J. Deng, J. Guo, N. Xue, and S. Zafeiriou, “Arcface: Additive angular margin loss for deep face recognition,” in *Proceedings of the IEEE/CVF conference on computer vision and pattern recognition*, 2019, pp. 4690–4699.

[67] C. Chen and J. Mo, “IQA-PyTorch: Pytorch toolbox for image quality assessment,” [Online]. Available: <https://github.com/chaofengc/IQA-PyTorch>, 2022.

[68] Z. Wang, J. Zhang, T. Chen, W. Wang, and P. Luo, “Restoreformer++: Towards real-world blind face restoration from undegraded key-value pairs,” *IEEE Transactions on Pattern Analysis and Machine Intelligence*, vol. 45, no. 12, pp. 15 462–15 476, 2023.

[69] S. Bai, K. Chen, X. Liu, J. Wang, W. Ge, S. Song, K. Dang, P. Wang, S. Wang, J. Tang *et al.*, “Qwen2. 5-vl technical report,” *arXiv preprint arXiv:2502.13923*, 2025.

[70] A. Radford, J. W. Kim, C. Hallacy, A. Ramesh, G. Goh, S. Agarwal, G. Sastry, A. Askell, P. Mishkin, J. Clark *et al.*, “Learning transferable visual models from natural language supervision,” in *International conference on machine learning*. PMLR, 2021, pp. 8748–8763.

[71] S. Fu, N. Tamir, S. Sundaram, L. Chai, R. Zhang, T. Dekel, and P. Isola, “Dreamsim: Learning new dimensions of human visual similarity using synthetic data,” *arXiv preprint arXiv:2306.09344*, 2023.

[72] X. Wu, Y. Hao, K. Sun, Y. Chen, F. Zhu, R. Zhao, and H. Li, “Human preference score v2: A solid benchmark for evaluating human preferences of text-to-image synthesis,” *arXiv preprint arXiv:2306.09341*, 2023.

[73] J. Hessel, A. Holtzman, M. Forbes, R. Le Bras, and Y. Choi, “Clipscore: A reference-free evaluation metric for image captioning,” in *Proceedings of the 2021 conference on empirical methods in natural language processing*, 2021, pp. 7514–7528.

[74] Y. Kirstain, A. Polyak, U. Singer, S. Matiana, J. Penna, and O. Levy, “Pick-a-pic: An open dataset of user preferences for text-to-image generation,” *Advances in neural information processing systems*, vol. 36, pp. 36 652–36 663, 2023.

[75] Y. Song, J. Sohl-Dickstein, D. P. Kingma, A. Kumar, S. Ermon, and B. Poole, “Score-based generative modeling through stochastic differential equations,” in *International Conference on Learning Representations*, 2021.

[76] C. Wu, J. Li, J. Zhou, J. Lin, K. Gao, K. Yan, S.-m. Yin, S. Bai, X. Xu, Y. Chen *et al.*, “Qwen-image technical report,” *arXiv preprint arXiv:2508.02324*, 2025.

[77] B. F. Labs, “Flux,” <https://github.com/black-forest-labs/flux>, 2024.

[78] J. Li, J. Cao, Y. Guo, W. Li, and Y. Zhang, “One diffusion step to real-world super-resolution via flow trajectory distillation,” *arXiv preprint arXiv:2502.01993*, 2025.

[79] T. Yin, M. Gharbi, R. Zhang, E. Shechtman, F. Durand, W. T. Freeman, and T. Park, “One-step diffusion with distribution matching distillation,” in *Proceedings of the IEEE/CVF conference on computer vision and pattern recognition*, 2024, pp. 6613–6623.

[80] Y. Song, P. Dhariwal, M. Chen, and I. Sutskever, “Consistency models,” 2023.

Zhengjian Yao received the B.S. degree in the School of Mathematics and Statistics from Xi'an Jiaotong University in 2022. He is currently pursuing the Ph.D. degree at the Medical Intelligence Lab, Peking University. His current research interests include low-level vision, applications of image generation, and reinforcement learning theories for large language models.



JiaKui Hu received the B.S. degree in School of Physics and Optoelectronic Engineering from Xidian University in 2023. He is currently pursuing the Ph.D. degree at Medical Intelligence Lab, Peking University. His current research interests include low-level vision and unified model.



Kaiwen Li received the Bachelor's degree in Electronic and Information Engineering from China University of Petroleum, Qingdao, China in 2021 and the Master's degree in Electronic science and technology from University of Electronic Science and Technology of China, Chengdu, China in 2024. He is currently pursuing the Ph.D. degree at Medical Intelligence Lab, Peking University. His current research interests include weakly supervised learning, image generation, and multimodal large language models.



Hangzhou He received the B.S. degree in Theoretical and Applied Mechanics from Peking University, Beijing, China in 2024. He is now a Ph.D. student majoring in Biomedical Engineering at Peking University. His research interests focus on the trustworthiness of deep learning models, including explainability, generalization and their applications in medical image analysis.





Xinlinag Zhang received the B.S. degree in Electronic Information of Engineering from Ocean University of China, Qingdao, China in 2021 and the Master degree in Computer Science and Technology from Tianjin University in 2024, Tianjin, China. He is now pursuing the Ph.D. degree at Medical Intelligence Lab, Peking University. His research interests include computer vision, deeplearning, and medical image analysis.



Shuang Zeng received a bachelor's degree in Engineering from Peking University, Beijing, China in 2021. He is currently a joint Ph.D. student of Peking University - Georgia Institute of Technology - Emory University Biomedical Engineering Program. His research mainly focuses on self-supervised contrastive learning and medical image processing.



Lei Zhu received the Ph.D. degree from Peking University, Beijing, China. He is currently a post-doc researcher at Medical Intelligence Lab, Peking University. His current research interests include weakly supervised learning, multimodal large language models, and medical image processing.



Yanye Lu is currently an Assistant Professor at Peking University. He was nominated by the Ministry of Education of China for the Young Changjiang Scholar Program in 2024. His research focuses on artificial intelligence (AI), computer vision, and multimodal medical imaging, with core interests in limited-supervision learning, robust and interpretable modeling, and multimodal generative AI. His work primarily targets the processing, analysis, and visualization of multimodal cross-scale biomedical information and medical images. He has published over 90 papers in top-tier journals across related fields (TPAMI, IJCV, TIP, TNNLS, TMI, MedIA, JNM) as well as in flagship computer science conferences including CVPR, ICCV, ICLR, NeurIPS, AAAI, and ECCV.

Supplementary Material

Bridging Information Asymmetry: A Hierarchical Framework for Deterministic Blind Face Restoration

TABLE OF CONTENTS

Appendix A: Derivation of the Re-balanced Objective	2
A-A Standard Bayesian Formulation	2
A-B Information Augmentation	2
A-C Preference Alignment via Energy-Based Models	2
A-D Final Objective	2
Appendix B: Discussion on Policy Gradient-based Diffusion RL	3
B-A Formulation of Policy Gradient on the Reverse Process	3
B-B Limitations for High-Fidelity Restoration	3
B-C Motivation for Adopting DiffusionNFT	3
Appendix C: Implementation Details of AR Prompting	3
C-A Multimodal Prompt Format	3
C-B Discrete Token Generation Logic	4
Appendix D: Details of Semantic Caption Generation	4
Appendix E: Evolution of Reward Scores on Validation Set	4
Appendix F: Implementation Details regarding Training Robustness	5
F-A Classifier-Free Guidance for Instruction Following	5
F-B Identity-Preserving Reconstruction Task	5
Appendix G: Additional Qualitative Comparisons	5
G-A More Results on CelebA-HQ	5
G-B Robustness on Real-World Degradation	8
G-C Holistic Structural Consistency vs. Local Artifacts	8
Appendix H: Discussion on the Distinction from Blip-3o Next	10
H-A Motivation: Generative Capability vs. Restoration Guidance	10
H-B Training Paradigm: Feature Alignment vs. Fine-grained Restoration.	10
H-C Optimization: Preference-Aware Space Pruning	11
Appendix I: Future Work and Limitations	11

APPENDIX A DERIVATION OF THE RE-BALANCED OBJECTIVE

In this section, we provide a probabilistic derivation for the objective function presented in Eq. 6 of the main paper. Our goal is to recover a deterministic high-quality image \hat{x} that is not only faithful to the degraded input y but also aligned with human perceptual preferences.

A. Standard Bayesian Formulation

In conventional blind image restoration, the problem is theoretically modeled as Maximum A Posteriori (MAP) estimation:

$$\hat{x}_{MAP} = \arg \max_x \log p(x|y) \quad (17)$$

$$= \arg \max_x (\log p(y|x) + \log p(x)) \quad (18)$$

where $p(y|x)$ is the likelihood term representing data fidelity, and $p(x)$ is the prior term capturing the statistics of natural images. However, as discussed in the main paper, due to the severe information loss in the degraded observation y , the posterior $p(x|y)$ is often highly uncertain with excessive entropy, leading to significant uncertainty in the restoration process.

B. Information Augmentation

To mitigate this uncertainty, we introduce an auxiliary variable \mathcal{S}_{AR} (the dense semantic integrator derived from our Auto-Regressive module). By conditioning the generative process on \mathcal{S}_{AR} , we seek to maximize the *augmented posterior* $p(x|y, \mathcal{S}_{AR})$. According to the fundamental property of conditional entropy (conditioning reduces entropy), we have:

$$H(x|y, \mathcal{S}_{AR}) \leq H(x|y) \quad (19)$$

The optimization objective for the generative backbone thus becomes:

$$\hat{x}_{aug} = \arg \max_x \log p(x|y, \mathcal{S}_{AR}) \quad (20)$$

This term corresponds to the standard training objective of our diffusion model, which learns to denoise conditional on both the degraded image and the text-derived features.

C. Preference Alignment via Energy-Based Models

While augmenting input information constrains the semantic content, the feasible solution space may still contain perceptually suboptimal artifacts (e.g., hallucinations or over-smoothing). To explicitly enforce human alignment, we model the human preference distribution as an Energy-Based Model (EBM), also known as a Boltzmann distribution:

$$p_{pref}(x) \propto \exp(\lambda \cdot \mathcal{R}_{pref}(x)) \quad (21)$$

where $\mathcal{R}_{pref}(x)$ is the scalar reward function learned from human preference data, and λ is a temperature coefficient controlling the strength of the constraint.

We interpret the final restoration goal as sampling from a *rectified posterior distribution* $q(x)$, which is proportional to the product of the augmented generative distribution and the preference distribution:

$$q(x|y, \mathcal{S}_{AR}) \propto p(x|y, \mathcal{S}_{AR}) \cdot p_{pref}(x) \quad (22)$$

Substituting the definition of $p_{pref}(x)$, we obtain:

$$q(x|y, \mathcal{S}_{AR}) \propto p(x|y, \mathcal{S}_{AR}) \cdot \exp(\lambda \mathcal{R}_{pref}(x)) \quad (23)$$

D. Final Objective

To obtain the optimal deterministic restoration result \hat{x} , we maximize the log-probability of this rectified posterior $q(x|y, \mathcal{S}_{AR})$:

$$\begin{aligned} \hat{x} &= \arg \max_x \log q(x|y, \mathcal{S}_{AR}) \\ &= \arg \max_x \left(\log \left[p(x|y, \mathcal{S}_{AR}) \cdot e^{\lambda \mathcal{R}_{pref}(x)} \right] \right) \\ &= \arg \max_x \left(\log p(x|y, \mathcal{S}_{AR}) + \log \left(e^{\lambda \mathcal{R}_{pref}(x)} \right) \right) \\ &= \arg \max_x (\log p(x|y, \mathcal{S}_{AR}) + \lambda \mathcal{R}_{pref}(x) + C) \end{aligned} \quad (24)$$

where C is a normalization constant independent of x . Ignoring the constant, this strictly corresponds to our proposed objective function in Eq. (1):

$$\hat{x} = \arg \max_x \left(\underbrace{\log p(x|y, \mathcal{S}_{AR})}_{\text{Augmented Likelihood}} + \lambda \cdot \underbrace{\mathcal{R}_{pref}(x)}_{\text{Preference Constraint}} \right) \quad (25)$$

This derivation demonstrates that our method can be theoretically viewed as searching for the mode of a posterior distribution that has been simultaneously *narrowed* by input augmentation and *modulated* by preference priors.

APPENDIX B DISCUSSION ON POLICY GRADIENT-BASED DIFFUSION RL

To further justify our selection of DiffusionNFT for deterministic face restoration, we provide a detailed discussion on traditional policy gradient methods for diffusion models, such as Group Relative Policy Optimization (GRPO) [27], [28].

A. Formulation of Policy Gradient on the Reverse Process

Recent works typically cast the reverse diffusion process as a Markov Decision Process (MDP) by discretizing the reverse Stochastic Differential Equation (SDE). Under the Euler–Maruyama scheme [75], the transition between adjacent timesteps is modeled as a tractable Gaussian policy:

$$\pi_\theta(x_{t-\Delta t} | x_t) = \mathcal{N}\left(x_t + \mathbf{f}_\theta(x_t, t)\Delta t, g_t^2 \Delta t \mathbf{I}\right), \quad (26)$$

where \mathbf{f}_θ is the drift term comprising the learned velocity v_θ . By formulating the sampling trajectory $\tau = \{x_T, \dots, x_0\}$ as a differentiable chain, policy gradient methods optimize the preference reward via:

$$\mathcal{L}_{\text{GRPO}}(\theta) = \mathbb{E}_{\tau \sim \pi_\theta} \left[\sum_t \log \pi_\theta(x_{t-\Delta t} | x_t) \cdot A(x_0) \right], \quad (27)$$

where $A(x_0) = r(x_0) - b(c)$ represents the advantage term, comparing the reward of a specific sample $r(x_0)$ against a baseline $b(c)$ derived from a group of samples.

B. Limitations for High-Fidelity Restoration

Despite their success in generative tasks, these reverse-process policy gradient methods face several critical bottlenecks when applied to the BFR task:

- 1) **Solver Dependency and Cumulative Error:** The optimization is tightly coupled to specific SDE solvers. Any mismatch between training discretization and inference sampling can lead to cumulative structural errors, which are fatal for identity-sensitive face restoration.
- 2) **Computational Overhead:** Calculating log-probabilities for the entire trajectory requires significant memory and limits the number of optimization steps, hindering the efficiency needed for fine-grained preference alignment.

C. Motivation for Adopting DiffusionNFT

In contrast, we adopt **DiffusionNFT** [29] because it shifts the reinforcement learning objective from the stochastic reverse process to the *deterministic forward process*.

DiffusionNFT offers three key advantages for our framework: (1) **Likelihood-free Optimization**: It eliminates the need for complex likelihood-ratio calculations, leading to more stable training; (2) **Solver Agnosticism**: It refines the underlying velocity field directly, making the restoration robust across different sampling schedules; and (3) **Negative-aware Contrast**: By explicitly modeling “low-reward” generations (e.g., hallucinations), it provides a clearer boundary to prune the solution space, which is essential for bridging the information gap between sparse LQ inputs and dense HQ outputs.

APPENDIX C IMPLEMENTATION DETAILS OF AR PROMPTING

A. Multimodal Prompt Format

To enable the Auto-Regressive (AR) model to switch between semantic understanding and image token generation, we adopt a specialized prompt format based on an expanded vocabulary. We introduce special tokens $\langle im_start \rangle$ and $\langle im_end \rangle$ as boundary markers for visual content.

For the image restoration task, the input prompt is structured as follows:

```
<|im_start|>user [Text Instruction] [LQ Visual Embeddings] <|im_end|>
<|im_start|>assistant <|im_start|>
```

B. Discrete Token Generation Logic

As shown in the format above, the suffixing of the second `<| im_start |>` at the end of the assistant's prefix serves as a *trigger signal*. During the Knowledge Alignment stage (Stage I), the model learns that this specific sequence must be followed by tokens from the visual vocabulary $\mathcal{V}_{img} = \{\langle I_0 \rangle, \dots, \langle I_{65535} \rangle\}$.

The generation process yields a sequence of N tokens (e.g., $N \in \{81, 169, 729\}$ depending on the selected scale), which are then reshaped and projected into the cross-attention layers of the Diffusion module. This mechanism ensures a deterministic transition from linguistic instructions to discrete structural priors.

APPENDIX D DETAILS OF SEMANTIC CAPTION GENERATION

To ensure high-quality and attribute-consistent semantic guidance during the training of the Auto-Regressive (AR) module, we utilized the **Qwen2.5VL-32B** model to generate detailed descriptions for the FFHQ training dataset. The prompt was meticulously designed to capture fine-grained facial attributes that are crucial for structural and identity-consistent restoration.

The specific system prompt used for image captioning is provided below:

“Please describe this portrait image in English. Start with ‘a photography of a’, incorporating descriptors such as gender, facial features, accessories, hairstyle, hair color, skin tone, and other characteristics you find relevant for depicting the person. Keep the description under 100 words.”

Rationale for Prompt Design:

- **Prefix Constraint:** By mandating the description to start with “*a photography of a*”, we maintain a consistent sentence structure across the entire dataset, which facilitates the AR module’s learning of the mapping between visual features and linguistic tokens.
- **Attribute Coverage:** Explicitly requesting descriptors such as *skin tone*, *accessories*, and *facial features* ensures that the generated captions provide the dense semantic anchors necessary to resolve ambiguities in severely degraded low-quality (LQ) inputs.
- **Length Constraint:** Limiting the output to 100 words ensures that the token sequence length remains within the efficient processing range of our AR integrator, avoiding excessive computational overhead while retaining sufficient descriptive power.

APPENDIX E EVOLUTION OF REWARD SCORES ON VALIDATION SET

To further validate the generalization and optimization efficacy of our Stage 2 preference-aware fine-tuning, we monitor the evolution of the compound reward score on a held-out validation set. This analysis provides insights into how the *Pref-Restore* model progressively aligns with human visual preferences and eventually surpasses existing state-of-the-art methods.

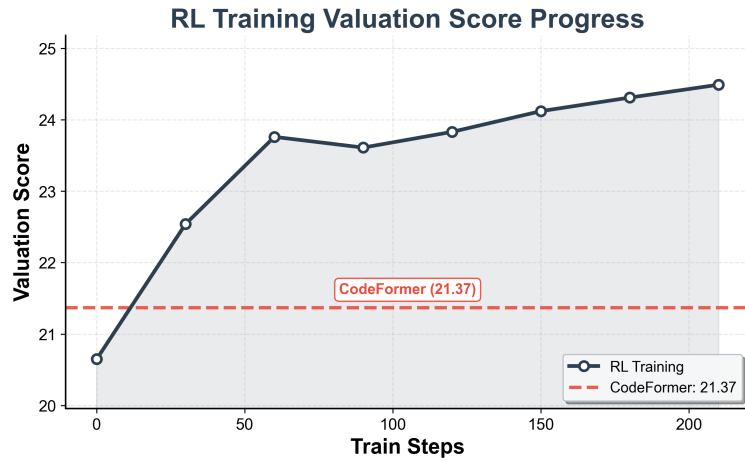


Fig. 9. **Progress of the compound reward score on the validation set during Stage 2 RL training.** The dashed red line indicates the performance of **CodeFormer** (21.37). Our *Pref-Restore* model (dark blue line) rapidly surpasses the baseline within the first 30 steps and consistently improves towards a plateau of 24.49, demonstrating superior alignment with high-quality perceptual priors.

Comparison with Competitive Baselines. As illustrated in Fig. 9, we plot the valuation score trajectory over 210 training steps. We select **CodeFormer** as a primary baseline, representing the current performance ceiling for deterministic face restoration methods. Initially, the base model (at step 0) starts with a valuation score of approximately 20.66, which is below the CodeFormer performance level of 21.37. However, as the DiffusionNFT optimization proceeds, the score exhibits a rapid

and robust ascent. By approximately the 30th training step, our model successfully surpasses CodeFormer, and it continues to climb, eventually plateauing at a high score of 24.49.

Analysis of the Optimization Curve. The steady growth and eventual stabilization of the validation score confirm several key aspects of our framework. **Effectiveness of RL Signals:** The significant gap between the final score (24.49) and the baseline (21.37) demonstrates that the RL-based preference alignment successfully explores the generative manifold to find solutions that are more "visually pleasant" than those produced by traditional pixel-wise or GAN-based objectives. **Convergence Stability:** The smooth transition from rapid growth to a stable plateau indicates a well-balanced learning rate and a robust gradient signal provided by the Forward Flow Contrast objective.

APPENDIX F IMPLEMENTATION DETAILS REGARDING TRAINING ROBUSTNESS

To ensure the versatility and fidelity of *Pref-Restore* in varied real-world scenarios, we incorporated two specific strategic designs during the data construction and training phases. These strategies aim to decouple the model's dependency on explicit textual instructions and enforce strict identity preservation under severe degradation.

A. Classifier-Free Guidance for Instruction Following

While our framework leverages textual descriptions to augment input information, real-world inference scenarios may not always provide user-specified prompts. To endow the model with the capability to support both text-guided and unconditional restoration, we adopted a stochastic prompt dropping strategy, inspired by Classifier-Free Guidance (CFG).

During the training phase, we dynamically construct the conversation template for the Auto-Regressive module. For each training sample, with a probability of $p_{txt} = 0.95$, we provide the explicit semantic instruction (e.g., "Please reconstruct the given image based on the image content: [Caption]"). Conversely, with a probability of $1 - p_{txt} = 0.05$, we supply a generic null-instruction prompt (e.g., "Please reconstruct the given image.") without specific semantic details. This randomized dropout prevents the model from over-relying on text embeddings and ensures robust performance even when textual guidance is absent or sparse during inference.

B. Identity-Preserving Reconstruction Task

In the context of Blind Face Restoration (BFR), achieving high fidelity in identity preservation is particularly challenging due to the severe loss of high-frequency details in LQ inputs. Relying solely on restoration from degraded inputs may cause the model to hallucinate plausible but identity-inconsistent features.

To explicitly reinforce the model's capability for faithful reconstruction, we introduced an auxiliary *Self-Reconstruction Task*. During the data loading pipeline, we apply a stochastic degradation bypass mechanism. Specifically, with a probability of $p_{rec} = 0.1$, the degradation process is skipped, and the ground-truth high-quality (HQ) image is directly used as the input "LQ" image. In this scenario, the task degenerates from an ill-posed restoration problem to a well-posed auto-encoding problem:

$$y_{input} = \begin{cases} x_{HQ}, & \text{if } \xi < p_{rec} \\ \mathcal{D}(x_{HQ}), & \text{otherwise} \end{cases} \quad (28)$$

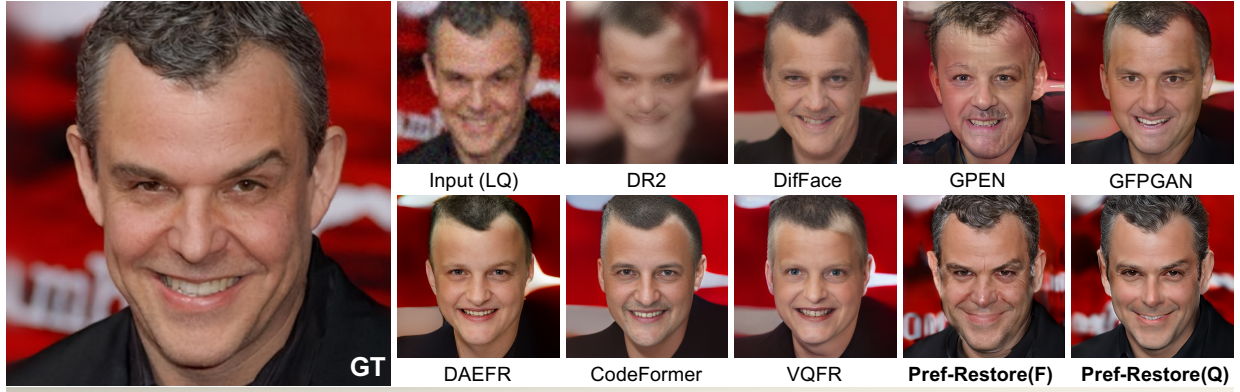
where $\xi \sim \mathcal{U}(0, 1)$. This strategy forces the network to learn an identity-to-identity mapping, effectively regularizing the feature space to retain the original structural integrity and preventing excessive generative deviations.

APPENDIX G ADDITIONAL QUALITATIVE COMPARISONS

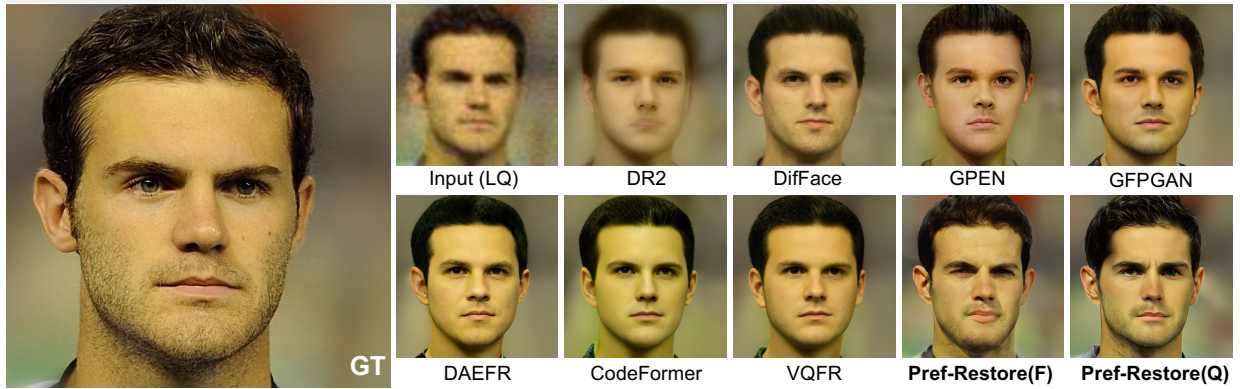
A. More Results on CelebA-HQ

In this section, we provide extensive qualitative comparisons on the CelebA-HQ dataset to further demonstrate the robustness and superiority of our *Pref-Restore* framework. As illustrated in Fig. 10 and Fig. 11, our method consistently outperforms state-of-the-art baselines across a wide range of facial attributes and environmental conditions.

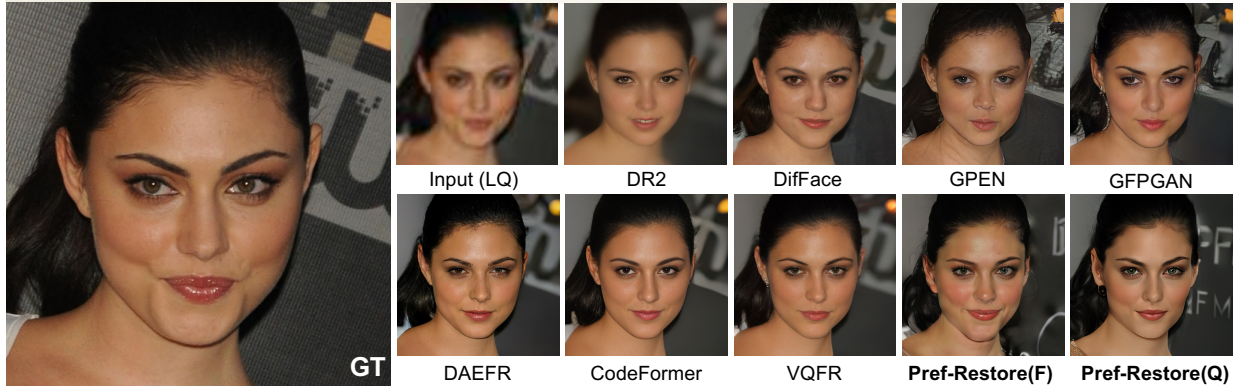
The results reinforce our core findings: *Pref-Restore(F)* effectively anchors the restoration process to the original facial manifold, preserving critical identity-defining features (e.g., specific eye shapes and hair structures) that are often lost in GAN-based or VQ-based methods. Simultaneously, *Pref-Restore(Q)* leverages preference-aware fine-tuning to suppress generative artifacts and restore high-fidelity textures, such as realistic skin pores and fine hair strands. Notably, in challenging scenarios involving complex backgrounds or diverse hairstyles, our framework maintains a superior balance between structural deterministic consistency and perceptual realism, successfully bridging the information asymmetry inherent in the BFR task.



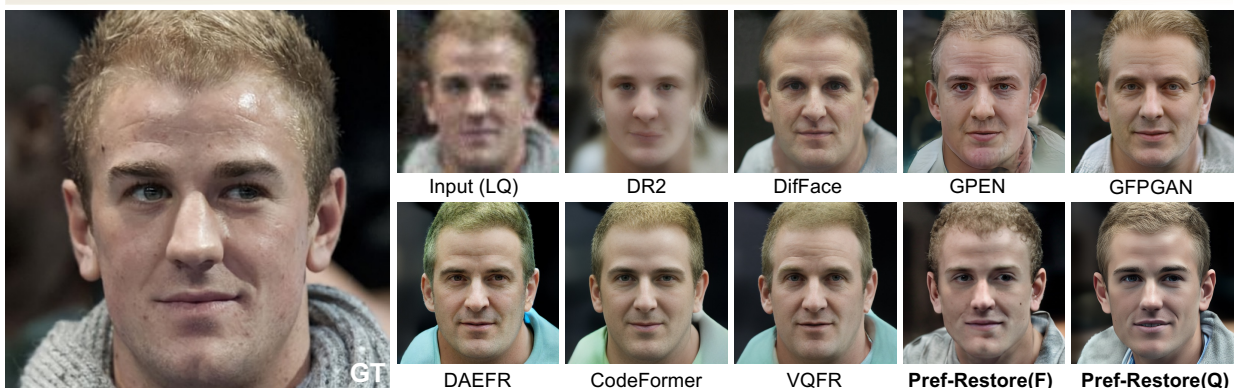
Caption: A photography of a person with short, wavy gray hair wearing a black jacket, set against a vibrant red backdrop.



Caption: A photography of a person with short, dark brown hair and a neatly trimmed beard.

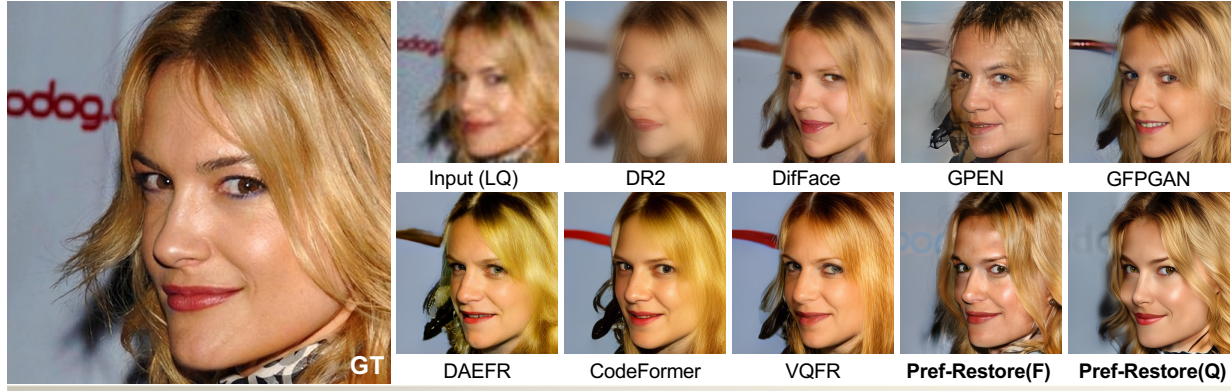


Caption: A photography of a person with long, dark hair, wearing a white top and standing against a pixelated backdrop.

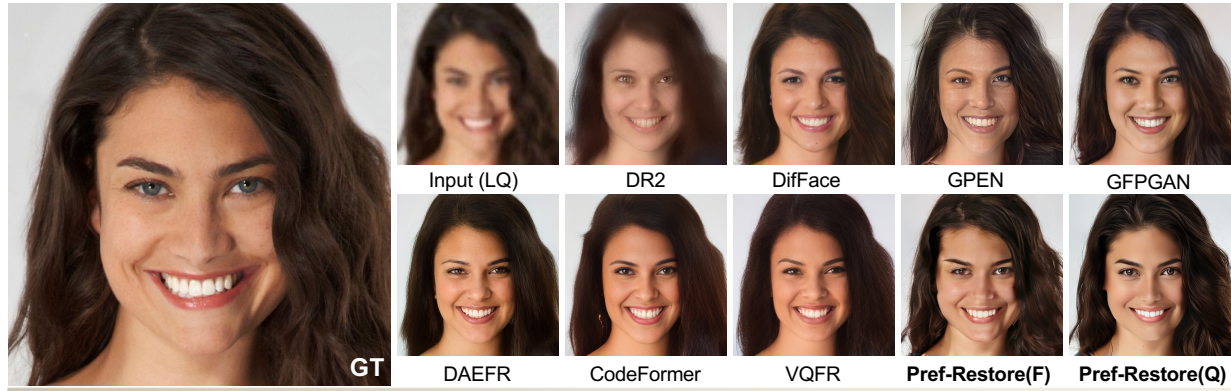


Caption: A photography of a person with short, light brown hair, wearing a gray sweater, against a dark background.

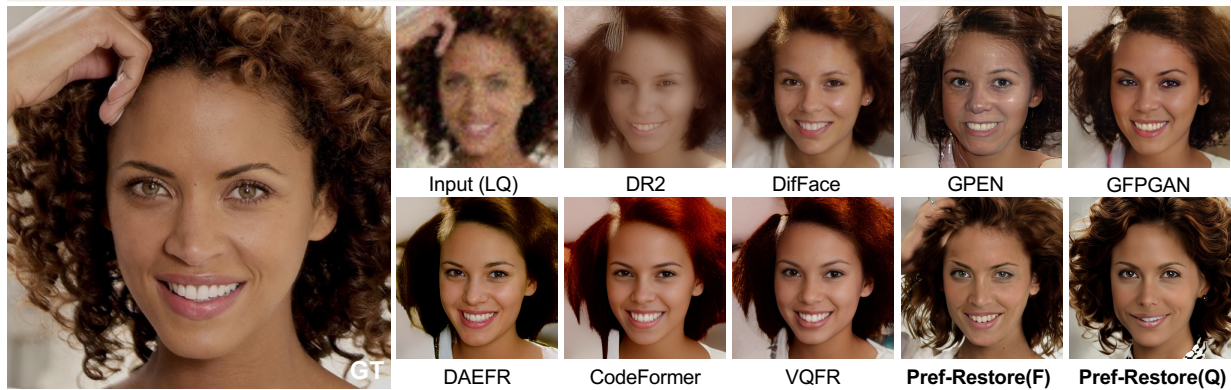
Fig. 10. Additional qualitative comparison on the CelebA-HQ dataset (Part I). Compared with SOTA methods, *Pref-Restore(F)* demonstrates superior structural anchors in preserving identity, while *Pref-Restore(Q)* achieves the highest perceptual quality. For instance, in rows with complex hair textures and diverse backgrounds, our framework avoids the over-smoothing common in *CodeFormer* and the identity-drift artifacts prevalent in diffusion baselines like *DifFace*.



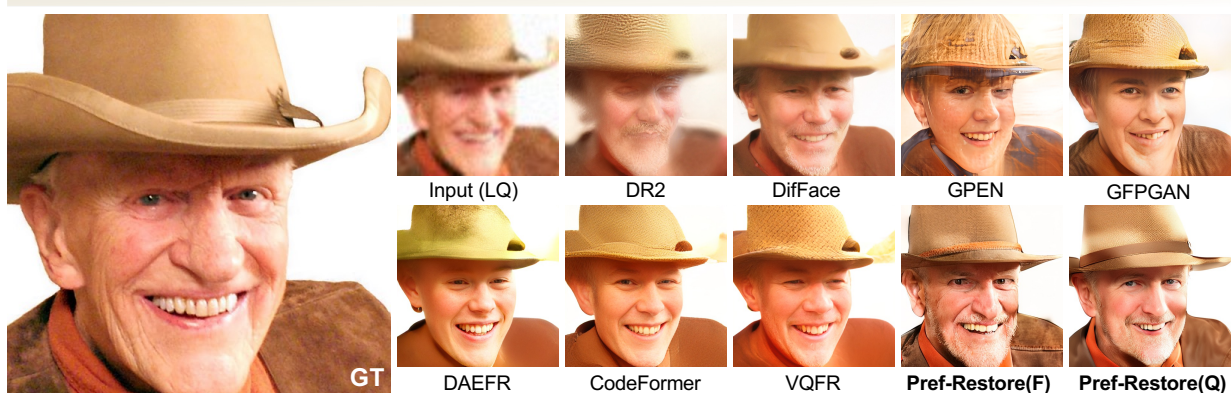
Caption: A photography of a person with long, wavy blonde hair against a backdrop featuring red text.



Caption: A photograph of a person with long, wavy dark hair against a plain background.



Caption: A photograph of a person with tightly curled brown hair and a hand touching their head.



Caption: A photography of a person wearing a large cowboy hat and a brown jacket.

Fig. 11. Additional qualitative comparison on challenging cases (Part II). This figure highlights our model's robustness against complex facial components and occlusions, such as tightly curled hair (row 3) and large accessories like cowboy hats (row 4). By internalizing solution boundaries through preference-aware fine-tuning, *Pref-Restore* eliminates stochastic uncertainty, yielding deterministic results that are both semantically plausible and identity-consistent.

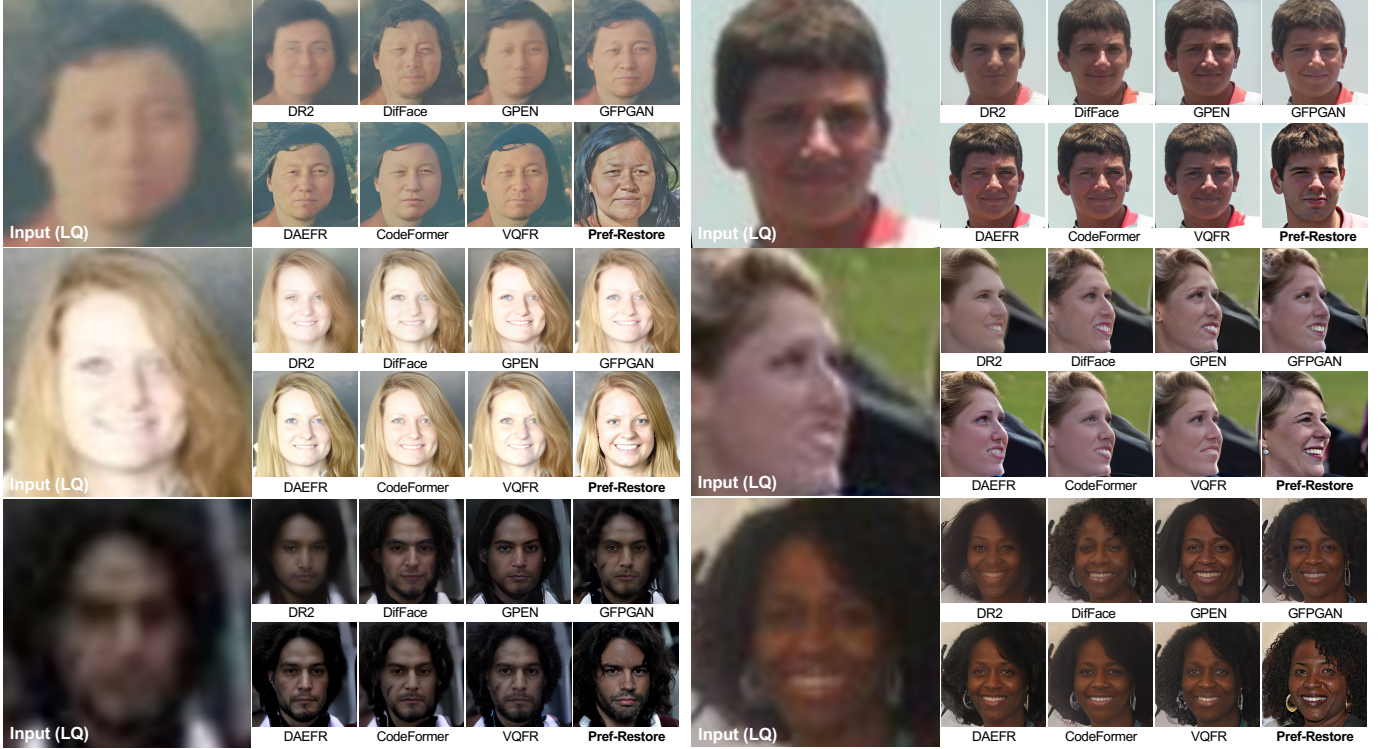


Fig. 12. **Qualitative comparison on real-world face degradation datasets.** Each row presents a challenging real-world case characterized by severe noise, blur, and low resolution. Our method, *Pref-Restore*, consistently produces the clearest and most structurally accurate results. Notably, while baseline methods often produce similarly over-smoothed or generic facial features due to potential overfitting on synthetic data, our framework leverages text-to-image priors to explore a more diverse and appropriate solution space, effectively restoring identity-consistent details even in extreme conditions.

B. Robustness on Real-World Degradation

To further evaluate the generalization capability of *Pref-Restore*, we provide additional qualitative results on real-world degraded face images, as shown in Fig. 12. Unlike synthetic datasets, real-world samples often contain complex, non-linear noise and unknown blur kernels that pose significant challenges to existing restoration models.

Our observations reveal two critical insights. First, *Pref-Restore* demonstrates exceptional clarity in scenarios with severe degradation. While competing methods often produce blurry or semantically ambiguous facial features under heavy noise, our framework consistently restores sharp edges and fine-grained textures (e.g., skin pores and hair filaments), yielding the most visually plausible results across all test cases.

Second, we observe a noticeable “convergence effect” among many baseline methods, where they tend to produce homogenized, overly-smooth outputs that lack distinct personal characteristics. We attribute this phenomenon to overfitting on the limited statistics of synthetic training data. In contrast, by leveraging the generative priors of large-scale text-to-image models, *Pref-Restore* is capable of navigating a much broader and more expressive solution space. This allows the model to find more accurate, identity-consistent solutions that align with the high-level semantic descriptions of the input.

C. Holistic Structural Consistency vs. Local Artifacts

A common limitation of existing BFR methods is their over-reliance on local texture restoration, which often leads to the neglect of global structural integrity and the introduction of unnatural artifacts. As illustrated in Fig. 13, our framework demonstrates superior holistic consistency by maintaining the geometric and anatomical plausibility of the entire image.

In case (a), we observe that while baseline models attempt to sharpen facial details, they significantly distort the shape of the hat, failing to preserve its realistic physical structure. This suggests that these models lack a global understanding of non-facial accessories, treating them as low-level textures rather than coherent objects. In contrast, *Pref-Restore* leverages AR-based semantic guidance to internalize the global context, ensuring that the restored hat retains its authentic, undistorted form.

In case (b), under extremely severe degradation, the limitations of local-focused restoration become even more apparent. Competing methods produce results with distorted eyeglasses or severe mismatches between the neck and the face—features that are anatomically incorrect for a human subject. These “hallucinated” artifacts arise because the models lack the hierarchical constraints necessary to align fine-grained textures with holistic structures. By synergizing high-level semantic reasoning with

preference-aware fine-tuning, *Pref-Restore* effectively eliminates such stochastic failures, yielding results that are both locally sharp and globally coherent.



Fig. 13. **Analysis of holistic structural consistency and global artifacts.** (a) Comparison of accessory restoration: Baseline methods often focus on local facial sharpness at the expense of global geometry, leading to warped and unrealistic hat shapes. (b) Restoration under extreme degradation: Baselines frequently produce anatomically inconsistent results, such as distorted eyeglasses and misaligned neck-face junctions. Our framework, *Pref-Restore*, maintains superior holistic integrity by integrating high-level semantic priors, ensuring that both facial and non-facial components are structurally plausible and free from global artifacts.

APPENDIX H

DISCUSSION ON THE DISTINCTION FROM BLIP-3O NEXT

While *Pref-Restore* leverages Blip-3o-Next as a foundational initialization, our framework is fundamentally distinct in terms of its motivation, training paradigm, and optimization objectives. This section clarifies these differences to highlight the necessity of our hierarchical design for the BFR task.

A. Motivation: Generative Capability vs. Restoration Guidance

The primary motivation of Blip-3o-Next is to harness the vast world knowledge and complex reasoning capabilities of Large Language Models to enhance the creative capacity of generative models. In contrast, *Pref-Restore* reformulates the role of the LLM as a provider of *auxiliary semantic stability*. We utilize textual priors not as a creative seed, but as high-level constraints to bridge the information asymmetry inherent in blind face restoration. Our framework uses the AR integrator to “reason” about missing facial components, converting sparse instructions into stable semantic anchors that guide the deterministic reconstruction process.

B. Training Paradigm: Feature Alignment vs. Fine-grained Restoration

The training of Blip-3o-Next focuses exclusively on the alignment between the LLM’s latent space and the Diffusion model’s textual space. Consequently, only the LLM parameters are fine-tuned, while the diffusion manifold remains largely unadjusted for specific reconstruction tasks.

As demonstrated in our ablation study (Sec. V-F) and the visualization in Fig. 14, this coarse-grained “Semantic-to-Diffusion Alignment” (represented by Stage 1.1 in the figure) is insufficient for high-fidelity restoration. While it aligns global features, it fails to recover identity-consistent textures. To address this, *Pref-Restore* introduces an additional **Texture-to-Diffusion Alignment** (Stage 1.2), which synchronizes VAE-encoded texture features with the generative manifold. As shown in the fourth column of Fig. 14, our full Stage 1 implementation achieves a significant leap in fidelity, validating that professional restoration requires more than just semantic feature mapping.

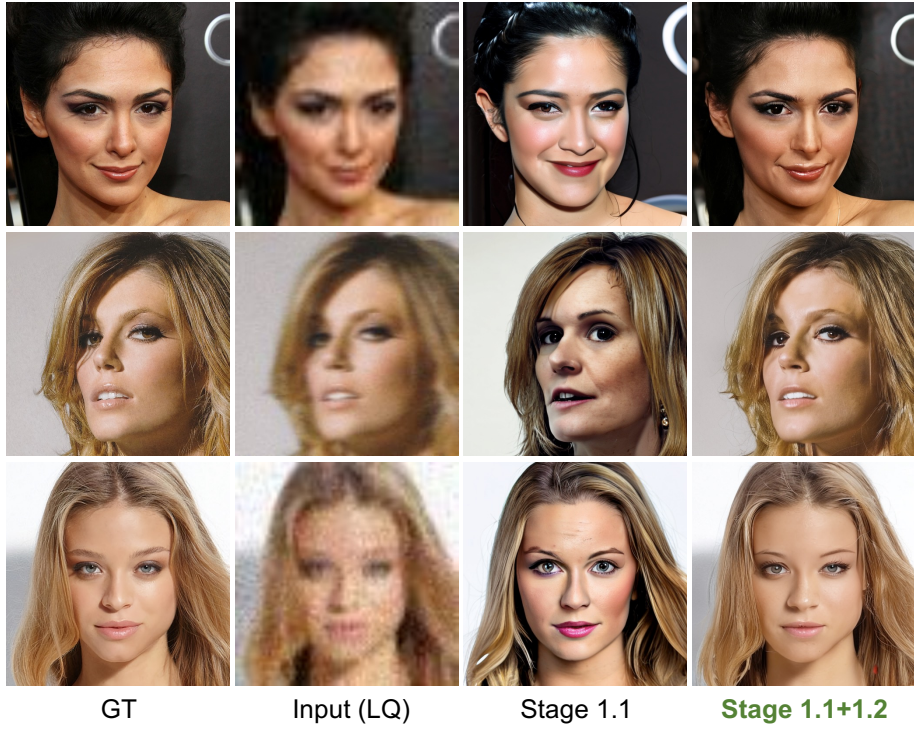


Fig. 14. **Visual comparison demonstrating the necessity of our hierarchical alignment.** The third column (Stage 1.1) illustrates the results using only *Semantic-to-Diffusion Alignment* (equivalent to the training paradigm of Blip-3o Next), where the lack of fine-grained structural constraints leads to identity inconsistency. The fourth column represents our full implementation, which incorporates *Texture-to-Diffusion Alignment* to achieve high-fidelity restoration.

C. Optimization: Preference-Aware Space Pruning

Finally, a key innovation of *Pref-Restore* is the integration of DiffusionNFT for preference-aware fine-tuning. While Blip-3o-Next excels in open-ended generation, it lacks a mechanism to constrain the solution space in image-conditioned tasks (e.g., image-to-image or face restoration). By incorporating on-policy RL, our framework internalizes human perceptual boundaries to prune suboptimal generative trajectories. This ensures the restoration is not only semantically plausible (as in Blip-3o) but also deterministic and rigorously aligned with human aesthetic and identity standards—a critical requirement for reliable face restoration that Blip-3o-Next does not address.

APPENDIX I FUTURE WORK AND LIMITATIONS

While *Pref-Restore* establishes a robust framework for deterministic blind face restoration, several avenues remain for future exploration to further enhance its scalability and efficiency:

a) Enhancing AR-based Semantic Guidance: Currently, the stability of textual instruction integration is somewhat constrained by the availability of high-quality multimodal restoration datasets and large-scale computational resources. Text-conditioned generative tasks typically require millions of data-text pairs to achieve flawless semantic alignment [76], [77]. Future work will focus on expanding the training corpus with more diverse facial descriptions and leveraging larger-scale pre-trained linguistic models to ensure even more stable semantic-to-visual mapping.

b) Diversifying Preference-Aware Rewards: In this work, we primarily utilized an aesthetic reward model to guide the RL process. However, the potential of DiffusionNFT to align with arbitrary human preferences remains largely untapped. Future research could investigate multi-dimensional reward functions that simultaneously optimize for identity preservation (e.g., via ArcFace-based rewards), lighting consistency, and even domain-specific artistic styles.

c) Enhancing Inference Efficiency: A practical limitation of the current framework lies in its inference latency, which is inherent to the iterative nature of diffusion-based sampling. While our method achieves superior fidelity, the computational cost may hinder real-time applications. We aim to explore algorithmic and engineering accelerations, such as consistency distillation or adaptive step-size solvers, to reduce the number of sampling steps without sacrificing the deterministic quality [78]–[80].